JCI The Journal of Clinical Investigation

Drug-regulated CD33-targeted CAR T cells control AML using clinically optimized rapamycin dosing

Jacob Appelbaum, … , Alexander Astrakhan, Michael C. Jensen

J Clin Invest. 2024. https://doi.org/10.1172/JCI162593.

Research In-Press Preview Hematology Therapeutics

Graphical abstract

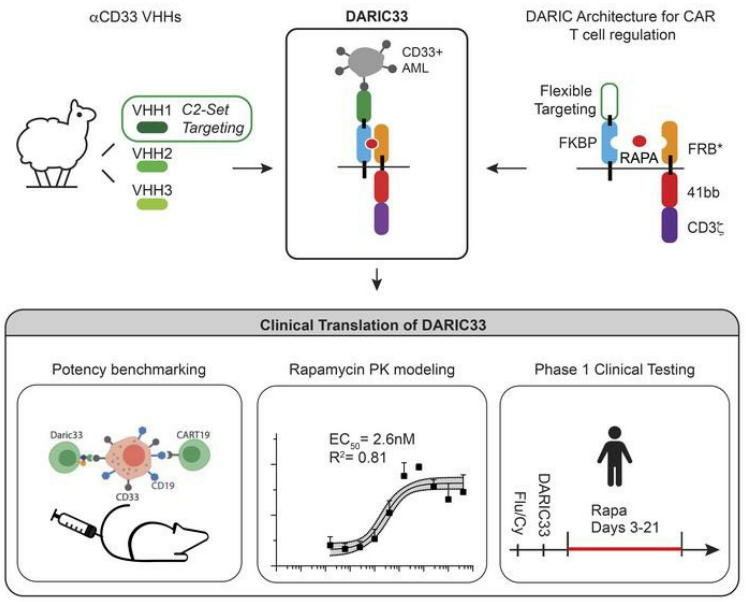

Title: Drug-regulated CD33-targeted CAR T cells control AML using clinically optimized rapamycin dosing

Authors: Jacob Appelbaum[1,2,3,4*], April E. Price[5], Kaori Oda[1], Joy Zhang[5], Wai-Hang Leung[5], Giacomo Tampella[1], Dong Xia[5], Pauline P. L. So[5], Sarah K. Hilton[5], Claudya Evandy[1], Semanti Sarkar[1], Unja Martin[5], Anne-Rachel Krostag[5], Marissa Leonardi[1], Daniel E. Zak[5], Rachael Logan[1], Paula Lewis[5], Secil Franke-Welch[5], Njabulo Ngwenyama[5], Michael Fitzgerald[1], Niklas Tulberg[1], Stephanie Rawlings-Rhea[1], Rebecca A. Gardner[1], Kyle Jones[6], Angelica Sanabria[6], William Crago[6], John Timmer[6], Andrew Hollands[6], Brendan Eckelman[6], Sanela Bilic[7], Jim Woodworth[7], Adam Lamble[1,4], Philip D. Gregory[5], Jordan Jarjour[5], Mark Pogson[5], Joshua A. Gustafson[1], Alexander Astrakhan[5*], Michael C. Jensen[1*]

Affiliations:

[1]Seattle Children's Therapeutics, Seattle Children's Research Institute; 1920 Terry Ave Seattle WA, 98101

[2]Division of Hematology/Oncology, Department of Medicine, University of Washington Medical School; 1705 NE Pacific Street, Box 357710 Seattle, WA 98195-7710

[3]Fred Hutchinson Cancer Center; 825 Eastlake Ave. E. Suite LG-700, Seattle, WA 98109

[4]Seattle Children's Hospital; 4800 Sand Point Way NE, MB.8.501, Seattle, WA 98105

[5]2Seventy bio; 60 Binney St. Cambridge MA 02142

[6]Inhibrx; Torrey Pines Science Park, 11025 N Torrey Pines Rd #200, La Jolla, CA 92037

[7]Vandro Consulting; Waukee, IA

*Corresponding authors:

Jacob Appelbaum, Fred Hutchinson Cancer Center, University of Washington, 825 Eastlake Ave E, Seattle WA 98109, jappelb@fredhutch.org

Sasha Astrakhan; 2seventy bio, 188 East Blane St Suite 300; Seattle WA 98102

sasha.astrakhan@2seventybio.com

Michael Jensen; BrainChild Bio; 1920 Terry Ave N, Seattle WA 98109

Michael.jensen@brainchildbio.com

Abstract: Chimeric antigen receptor (CAR) designs that incorporate pharmacologic control are desirable, however designs suitable for clinical translation are needed. We designed a fully human, rapamycin-regulated, drug product for targeting CD33+ tumors called dimerization agent regulated immunoreceptor complex (DARIC33). T cell products demonstrated target specific and rapamycin-dependent cytokine release, transcriptional responses, cytotoxicity, and in vivo antileukemic activity in the presence of as little as 1nM rapamycin. Rapamycin withdrawal paused DARIC33-stimulated T cell effector functions, which were restored following re-exposure to rapamycin, demonstrating reversible effector function control. While rapamycin-regulated DARIC33 T cells were highly sensitive to target antigen, CD34+ stem cell colony forming capacity was not impacted. We benchmarked DARIC33 potency relative to CD19 CAR T cells to estimate a T cell dose for clinical testing. In addition, we integrated in vitro and preclinical in vivo drug concentration thresholds for OFF-ON state transitions, as well as murine and human rapamycin pharmacokinetics, to estimate a clinically applicable rapamycin dosing schedule. A phase 1 DARIC33 trial has been initiated (PLAT-08, NCT05105152), with initial evidence of rapamycin-regulated T cell activation and anti-tumor impact. Our findings provide

evidence that the DARIC platform exhibits sensitive regulation and potency needed for clinical application to other important immunotherapy targets.

Main Text:

INTRODUCTION

Chimeric antigen receptor (CAR) T cell products are potent living drugs that dramatically expand in the days following adoptive transfer into patients. For existing CD19 and BCMA CAR T cell products, T cell engraftment, expansion, function, and persistence characteristics are product autonomous, such that, at their peak, CAR T cells may number 100- to 1000-fold greater than the number of cells initially infused (1). Toxicities, such as cytokine release syndrome (CRS), immune effector cell associated neurotoxicity syndrome (ICANS), and rare late effects, such as marrow hypoplasia, have also been reported (2). Technologies that allow physicians to control the activity of engineered T cell therapies following patient infusion may address some of the safety concerns associated with this promising class of drugs.

In many applications, such as acute myeloid leukemia (AML) and solid tumors, on-target/off-tumor product reactivity may negatively impact therapeutic index. In the case of B-cell malignancies, broad targeting and elimination of both normal and malignant CD19+ cells is generally well tolerated and clinically manageable. However, in the case of AML, no known target allows selective ablation of malignant myeloid cells without the simultaneous loss of essential nonmalignant cell types (3). Despite this caveat, hematopoietic stem/progenitor cell (HSPC) antigens with increased expression on AML blasts, such as CD33, CD123 and CLL1 (CLEC12A) have emerged as potential targets. Thus, targeting AML antigens with constitutively active CAR T cell products may eliminate HPSCs, resulting in prolonged or permanent marrow hypoplasia. A technological platform that allows for recursive cycles of tumor kill interspersed

with periods of myeloid recovery, akin to cycles of cytotoxic chemotherapy, is a conceptually attractive approach to target this class of AML antigens.

Drug-induced dimerization of split CAR designs may be a general approach to allow physicians to modulate CAR activity in a time scale matched to clinical need. Previously reported dimerizing agent-regulated immunoreceptor complexes (DARICs) are composed of separate antigen targeting and T cell signaling components, with embedded extracellular rapamycin-dependent heterodimerizing domains (4). Targeting and signaling components dimerize in the presence of rapamycin, resulting in antigen-responsive T cell activation (4, 5). Prior studies demonstrated that CD19-targeted DARIC T cells (DARIC19) display OFF to ON (e.g. quiescent to antigen responsive) functional transitions in the presence of sub-immunosuppressive concentrations of rapamycin (e.g. $\leq$ 1 nM), well below the range recommended for immunosuppression in patients following solid organ transplant (6). Further, DARIC19 T cells in the presence of nanomolar concentrations of rapamycin exhibited potency equivalent to conventional CD19 CAR T cells in preclinical in vitro and in murine disease models.

Here, we describe the assembly and validation of a CD33 targeted DARIC chimeric immunoreceptor. From a single domain V_HH antibody library, we identified candidate CD33-binders that redirect T cell effector functions to target cells expressing CD33, an established AML antigen (7). Among several high affinity single domain antibodies, we identified one candidate capable of recognizing an epitope within the membrane proximal C2-set domain of CD33, which is a conserved domain across CD33 splice isoforms (8). DARIC receptors incorporating the C2 epitope-specific V_HH (DARIC-V_HH1) displayed rapamycin-dependent recognition and activation against multiple gene modified and AML cell lines, as well as an in

vivo antitumor effect against established CD33+ human tumor xenografts in NSG mouse models. Following manufacture of clinical scale DARIC33 T cell lots using GMP manufacturing methodologies, we found donor-matched DARIC33 T cells and control CD19 CAR T cells both exhibited similar expression of phenotypic markers associated with engraftment fitness while neither expressed markers associated with tonic signaling or exhaustion. Finally, correlation of dose-exposure and activity relationships establish rapamycin concentration thresholds required for DARIC33 T cell activity in vivo. Based on these findings, we have initiated a phase I DARIC33 trial in pediatric patients with relapsed/refractory AML and demonstrated initial signs of rapamycin-mediated T cell activation and tumor response. Together, these observations will serve as a model for the development of additional drug-regulated T cell therapies.

RESULTS

The DARIC architecture utilizes a split CAR design in which the antigen targeting and T cell signaling domains are separated into distinct transmembrane receptors that contain extracellular cognate rapamycin-dependent heterodimerization domains (**Fig. 1A**). This bipartite design leverages a highly energetically favorable ternary complex between rapamycin and the rapamycin binding domains derived from *FK506-binding protein 12kd (FKBP12)* and mammalian target of rapamycin (mTOR) *FKBP12-rapamycin-binding (FRB)* domain. The FRB domain was modified to incorporate the T2098L mutation, which destabilizes domain folding in the absence of rapamycin and increases the rate of protein turnover(9), promoting a stringent off state. We previously reported potent and reversible rapamycin-dependent anti-tumor responses by CD19-DARIC T cells (4) and sought to adapt this design for an AML therapeutic approach by engineering the DARIC to target CD33.

Construction of rapamycin-dependent CD33-targeted DARICs

To identify CD33-targeting single domain antibodies, a library screen of heavy chain only (V_HH) binders isolated following alpaca immunization and yeast surface display was conducted. Three lead V_HH candidates that bound recombinant human CD33 protein were identified. To confirm hits, binders were tested against CHO cells transiently expressing CD33 using increasing amounts of purified recombinant anti-CD33 V_HH-Fc fusion proteins and secondary antibodies. Evaluation of binding isotherms revealed apparent affinities ranging from 0.9nM to 249nM (**Fig. S1A**). The binding characteristics of clone V_HH1 were further characterized by surface plasmon resonance (SPR) (**Fig. S1B**).

To determine whether CD33 specific V_HH domains are capable of redirecting DARIC T cell effector functions, codon optimized V_HH domains were embedded as the targeting moiety of the DARIC architecture, resulting in DARIC-V_HH1-3 (4). Peripheral blood mononuclear cells (PBMCs) were activated with CD3/CD28 antibodies, transduced with lentiviral vectors and expanded for *in vitro* analysis (**Fig. 1B**). T cell products contained an average of 1.5 to 2 integrated lentiviral genomes per cell, independent of construct (**Fig. S1C**). Untransduced (UTD) T cells, both in the presence or absence of rapamycin, exhibited low to undetectable levels of interferon gamma (IFNγ) release following coculture with CD33+ tumor cells in media with and without rapamycin (Fig. 1C), reflecting minimal T cell activation. In addition, while none of the DARIC-V_HH T cell products responded to CD33+ stimulator cells in the absence of rapamycin each produced 120 – 240 μg/mL IFNγ when 1nM rapamycin was added to the coculture, an increase of 50-74-fold above UTD cells (**Fig. 1C**). This data demonstrates that DARIC-V_HH T cells are stringently dependent on rapamycin for effector cytokine release.

Rapamycin stabilizes the surface expression of DARIC components.

The FRB domain has been shown to act as a rapamycin sensitive degron (10). Therefore, we assessed the effect of rapamycin exposure on surface expression of both targeting and signaling polypeptide receptors on DARIC-V_HH T cells. Following incubation of DARIC-V_HH T cells in standard media or media containing 1nM rapamycin, we evaluated surface expression of DARIC-V_HH components using flow cytometry by staining cells with biotinylated CD33 antigen, anti-FRB, or anti-V_HH antibodies. Across all DARIC-V_HH constructs, rapamycin exposure increased the proportion of T cells binding soluble CD33 antigen by 26%-38% (ANOVA $p = 0.0232$), and the mean fluorescence intensity (MFI) by 2-4 fold (ANOVA $p < 0.0001$) (**Fig. 1D**). We also observed increased surface expression of both FRB and V_HH domains after rapamycin exposure (ANOVA $p < 0.001$, **Fig. 1E, F**). While the percentage of DARIC+ cells diverged among the various detection methods, the MFI ratio with +/- rapamycin were similar with all analytic approaches. In addition and similar to DARIC19 (4), these results demonstrate that rapamycin increases surface expression of DARIC33 components to facilitate T cell responses.

DARIC-V_HH T cells are sensitive to low levels of rapamycin and CD33 antigen.

To determine rapamycin concentration thresholds required for DARIC-V_HH T cell activation, we assayed cytokine release from 24 hour co-cultures of DARIC-V_HH T cells and CD33+ AML target cells, including a rapamycin concentration range up to 4 nM (**Fig. 2A**). Release of IFNγ and IL-2 followed a sigmoidal response to increasing rapamycin concentrations, reaching a maximum in the presence of 0.25 nM rapamycin and remaining unchanged at higher rapamycin concentrations. DARIC-V_HH2 induced more cytokine release than the other two V_HH clones.

The rapamycin EC_{50} for DARIC-V_HH T cell activation, determined by cytokine release, ranged from 15.8 pM to 74.2 pM for IFNγ and IL-2 (**Fig. 2A**), and 17 pM to 52 pM for TNFα (**Fig. S2A**). Based on these data, the rapamycin concentration required for DARIC-V_HH T cell activation in the presence of CD33+ target cells is near or below the IC_{50} of mTORC1 (62 pM) or mTORC2 (534 pM)(11).

We next assessed CD33 antigen sensitivity by co-culturing DARIC-V_HH T cells with target cells expressing a range of CD33 antigen densities in the presence or absence of rapamycin. HEK293T cells electroporated with escalating amounts of CD33 mRNA exhibited dose-dependent levels of cell surface CD33 protein as determined by flow cytometry (**Fig. S2B**). In the presence of rapamycin and target cells with increasing CD33 antigen density, IFNγ release by DARIC-V_HH T cells increased between 19 and 140-fold and IL-2 release increased between 408 and 618-fold (**Fig. 2B**). Among samples treated with CD33 mRNA, CD33 expression increased 38-fold, while IFNγ release by DARIC-V_HH T cells increased only 2- to 3-fold, suggesting saturation of DARIC-V_HH signaling outputs at low densities of CD33. We further evaluated rapamycin-dependent induction of IFNγ release following stimulation of DARIC-V_HH T cells by target cells expressing lower densities of CD33 (**Fig. S2D,E**). One construct, DARIC-V_HH2, released substantial amounts of IFNγ in the presence of rapamycin and unmanipulated HEK293T cells, suggesting antigen-independent signaling of this construct (**Fig 2B** and **Fig S2E**). Addition of soluble CD33 protein to coculture experiments did not inhibit rapamycin-dependent DARIC33 stimulation of T cell responses (**Fig. S2F**). Together these results demonstrate rapamycin-activated DARIC-V_HH T cells exhibit sensitivity to AML target cells with low CD33 densities.

DARIC-V_HH T cells exhibit rapamycin-dependent antileukemic activity in vivo.

To evaluate anti-tumor activity in vivo, we used xenograft tumor models in which immunodeficient NSG mice are intravenously inoculated with luciferase-tagged AML cell lines in the context of a range of rapamycin doses and administration schedules. MOLM14, a cell line derived from a secondary AML, exhibits robust CD33 expression (**Table S1**) and, following modification for bioluminescence imaging (BLI), grows rapidly when inoculated into NSG mice. Following intravenous inoculation of MOLM14 AML cells, we treated mice with DARIC-V_HH or UTD control T cells followed by rapamycin delivered at a dose of 0.1mg/kg by intraperitoneal (IP) injection three times weekly for the duration of the study (**Fig. 2C**). Mice treated with UTD T cells demonstrated logarithmic increases in tumor burden and developed tumor associated symptoms within 3 weeks (**Fig. 2D**). Mice treated with DARIC-V_HH T cells without rapamycin exhibited equally rapid tumor progression. In contrast, mice treated with DARIC-V_HH T cells and rapamycin displayed delayed tumor growth and significantly extended survival.

As a second xenograft tumor model to evaluate DARIC-V_HH anti-tumor activity, we used the CD33-expressing acute promyelocytic leukemia-like cell line HL60, modified for BLI j(**Fig. 2E**). We similarly observed DARIC-V_HH T cell anti-tumor activity that was fully rapamycin dependent (**Fig. 2F**). None of the mice in either HL60 or MOLM14 models lost weight following adoptive transfer of DARIC-V_HH T cells, either alone or followed by rapamycin administration (**Fig. 2F** and data not shown). Across both AML tumor models, the rank order of anti-tumor activity exhibited by the DARIC-V_HH constructs was preserved. Together, these studies demonstrate that the DARIC-V_HH chimeric immunoreceptor architecture elicits *in vivo* anti-tumor activity in the presence of rapamycin.

DARIC-V_HH1 T cell activation is specific to the membrane proximal domain of CD33

Because alternative splicing impacts CD33 expression (8, 12, 13), we included cDNAs encoding both full length CD33M and the major alternative shorter transcript CD33m, which lacks the membrane distal Ig-like IgV2 sialic acid-binding domain encoded by exon 2 (14–16) in our screening library. Expression of CD33M resulted in a strong fluorescent signal following staining with all three V_{HH}-Fc fusion proteins, while expression of CD33m resulted in a strong fluorescent signal only following staining with V_HH1-Fc (**Fig. S1A and S3A**). To verify the CD33 membrane proximal epitope specificity we stained CHO cells transiently expressing CD33m with increasing concentrations of purified V_HH-Fc fusions and secondary antibodies. V_HH1-Fc fusion bound CD33m expressing CHO cells with an apparent K_d = 162 nM, whereas no binding of V_HH2Fc or V_HH3Fc to CD33m was detected (**Fig. S3A**).

To evaluate potential off-target activity, we screened CD33-targeting V_HH domains for binding to a library of transgenes encoding 5,528 secreted and transmembrane proteins. HEK293T cells expressing library transgenes were spotted on slides, fixed, and stained with anti-CD33 V_HH domain-Fc protein fusions followed by fluorescently labeled anti-Fc secondary antibodies (**Fig. 3A**). This screen did not identify strong binding of the CD33-specific V_HH clones to non-CD33 cell surface molecules in the library. We did observe weak fluorescent signal of V_HH1 towards samples expressing Siglec-6 (NM_198845), a sialic acid binding protein recently identified as a potential antigen target for AML (17) that shares substantial homology with CD33. We also observed weak V_HH3 reactivity towards MMP13 (**Fig. 3B**).

To determine whether DARIC-V_HH1 T cells respond to CD33m or Siglec-6, we cultured DARIC T cells with HEK293T cell lines electroporated with CD33M-, CD33m-, or Siglec6-encoding mRNA (**Fig. 3C-D**). Consistent with the findings above, DARIC-V_HH1 T cells

exhibited rapamycin-dependent IFNγ release following coculture with HEK293T cells expressing CD33M or CD33m, whereas T cells expressing DARIC-V_HH3 T cells responded only to HEK293T cells expressing CD33M (**Fig. 3C**). Similarly, we cultured DARIC-V_HH1 or DARIC-V_HH3 T cells with HEK293T cells, electroporated with titrated amounts of Siglec-6 mRNA, in the presence or absence of rapamycin (**Fig. 3D**). When rapamycin was present, HEK293T cells electroporated with the highest amounts of Siglec6 mRNA stimulated release of 40-60 ng/mL IFNγ from DARIC-V_HH1 T cells, which corresponds to approximately 10% of the amount released following coculture with CD33+ AML cells. No IFNγ release was observed when DARIC-V_HH1 T cells were cultured with HEK293T cells expressing lower levels of Siglec-6. Transgenic expression of CD33 in lung cancer cells that do not endogenously express CD33 **(Fig S3B)** resulted in rapamycin-dependent DARIC-V_HH1 T cells proliferation *in vitro*, whereas targeted deletion of CD33 from CD33+ AML cell lines eliminated IFNγ responses *in vitro* (**Fig. S3C-D**) and *in vivo* (**Fig. S3G**) In addition, DARIC-V_HH1 T cells exhibited anti-tumor activity in a $CD33^{low}$ Nalm6 xenograft tumor models (**Fig. S3E-F**). Together, these data show that stimulation of T cell effector functions by DARIC-V_HH1 is specific to the membrane proximal domain of CD33 present in both CD33M and CD33m isoforms. The strict target specificity, promising affinity characteristics, rapamycin dependence, and recognition of both CD33M and CD33m led us to select DARIC-V_HH-Clone 1 as a lead clinical candidate for subsequent development. Below, we refer to DARIC-V_HH1 simply as DARIC33, and T cell products manufactured by Seattle Children's Therapeutics at clinical scale using good medical practice (GMP) compatible reagents and techniques as SC-DARIC33.

CD33m is a prevalent isoform of CD33 expressed by AML

Four separate single nucleotide polymorphisms (SNPs) have been reported to influence splicing of CD33 by SRSF2(14, 16), including rs12459419 C>T in the splice enhancer region that regulates exon 2 skipping and rs2455069 A>G resulting in protein modification (14–16). Though controversial (18), the rs12459419 T/T genotype has been associated with predominance of the shortened transcript (lacking exon 2) encoding CD33m, and poor responses to CD33-targeted therapeutics that recognize the IgV2 domain missing from CD33m (14, 19). We reviewed transcriptional profiles of 577 AML cases, evaluating the proportion of CD33 transcripts lacking exon 2. We identified strong correlations between SNPs and CD33m transcript expression among AML cases (**Fig. S4A-E**). We also identified CD33m transcripts among profiles of healthy tissues, though with less abundance than among AML cases (**Fig. S4F**). While attempts at targeting the CD33m isoform for AML immunotherapy are being developed (20, 21), these strategies have also faced challenges. As a potential control, some studies have shown that antibody HIM3-4 is specifically reactive to the CD33m isoform, we observed minimal reactivity of this clone towards CD33m over-expressing cells (**Fig. S4G**). Coculture of DARIC33 T cells with AML cells of various rs12459419 SNP genotypes (21, 22) including OCI-AML3 (T/T), U-937 (C/C), HL-60 (C/C), MV4-11 (C/T), and MOLM14 (C/C) stimulated similar rapamycin-dependent release of IFNγ and IL-2(**Fig. 3E**), despite different CD33M expression density (assessed using IgV2-targeted p67.6 antibody, see **Supplemental Table S1**). Combined, these findings demonstrate the challenges associated with targeting the CD33m epitope with established antibody clones and support the use of DARIC33 to target $CD33^+$ cells across a range of expression and isoform usage.

DARIC33 T cells do not impact hematopoietic colony forming capacity.

CD33 is expressed by granulocyte precursors (23) as well as hematopoietic stem/progenitor cells (HSPC) with potential for multilineage engraftment in immunodeficient mice (24). Elimination of HSPC may result in intolerable myeloablation (25, 26). However, recent studies found the number of cells with the potential to form multilineage colonies in stem cell plating assays is not decreased by exposure to CD33 CAR T cells (27). To assess hematopoietic safety of DARIC33, we plated purified CD34+ HSPCs in colony forming assays following overnight incubation alone or together with a 10-fold excess of DARIC33 cells or comparator T cell products and rapamycin. As expected, colony forming units (CFU) of the granulocyte/monocyte lineage (CFU-GM) and of multilineage precursors (CFU-GEMM) were markedly reduced following incubation with CD123 CAR T cells (28), but not following incubation with UTD control cells (**Fig. 3F**). Compared to UTD T cells, the number of CFU-GM and erythroid burst forming units (BFU-E) were slightly reduced following coculture with DARIC33 effector T cells in the presence of rapamycin, but not when rapamycin was omitted from the overnight culture. These data suggest that while activated DARIC33 T cells have some impact on hematopoietic colony formation, this is a rapamycin-dependent process that can be controlled by withdrawing the drug.

Rapamycin exposure drives an antigen-dependent CAR T cell activation signature in DARIC33 T cells.

Transcriptional programs are tightly associated with T cell differentiation and functional status (29, 30). We interrogated transcriptional changes of sorted CD4+ and CD8+ DARIC33 cells following antigen exposure in the presence or absence of rapamycin (see **Fig. 4A** for

schema). We then modeled transcriptional changes to identify a "DARIC active" profile distinct from either "antigen without rapamycin" or "rapamycin-only" transcriptional profile, restricting our analysis to a subset of genes informative of changes in T cell states (see Supplemental Methods). Of the 2,792 queried genes, 228 genes showed transcriptional regulation specific to the *DARIC active* condition in either the CD4 or the CD8 population, or both (genes with FDR < 0.05 and fold change > 2.8 over the combined individual effects of rapamycin and antigen, **Fig. 4B,** see also **Fig. S5**). Following rapamycin exposure and antigen stimulation, DARIC33 cells transcriptional profiles showed significant enrichment of CAR T cell activation genes (Fisher exact test; CD4 $p = 0.024$ and CD8 $p = 0.005$), including *GZMB*, *IL2RA* and *TNFRSF9* (encoding 4-1BB) (**Fig. 4C**), which was also reflected by changes in protein abundance as measured by flow cytometry (**Fig. 4D**). Taken together, these results reveal a transcriptional activation signature of DARIC33 CD4+ and CD8+ T cells in the presence of both target antigen and rapamycin. Notably, this signature is consistent with conventional CAR T cells activated by antigen in the absence of rapamycin (31–33).

DARIC33 and CAR33 T cells have similar functionality and activation signature.

We have previously shown equivalent functional activity when the same CD19-targeting scFv was placed in either a CAR vs a DARIC backbone (4). To investigate whether DARIC33 T cells had similar activity as a CAR, we generated CD33-targeting CAR T cells using the identical CD33-specific V_HH1 binder. Both CAR33 and DARIC33 T cells had similar expression and virus integration profile (**Fig S6A**). When co-cultured with CD33+ HL60 tumor cells, CAR33 T cells had robust IFNγ production in the presence or absence of rapamycin, while DARIC33 only secreted cytokines in the presence of rapamycin (**Fig S6B**). In addition, both CAR33 and rapamycin-exposed DARIC33 T cells had similar rates of cytotoxicity in vitro (**Fig**

S6C). Next, we analyzed the phenotype of both CAR33 and DARIC33 T cells with or without activation. We observed some evidence of tonic signaling in the CAR33 T cells, characterized by increased CD69 and CD25 expression compared to unstimulated DARIC33 T cells (**Fig. S6D-E**). Following co-culture with CD33+ tumor cells, both CAR33 and DARIC33 T cells exhibited a similar activation profile, however the CAR33 cells had higher expression of PD1, LAG3, CD69 and CD25, suggesting greater activation following T cell activation (**Fig. S6D-E**). Together, these data suggest similar rates of tumor reactivity for both CAR33 and DARIC33 platforms, with the DARIC33 cells demonstrating lower rates of tonic signaling compared to the CAR33 platform.

GMP manufacturing at scale generates SC-DARIC33 cell products with similar features as CD19 CAR T cell products.

To evaluate the performance of DARIC33 generated at clinical scale (SC-DARIC33), we generated donor-matched (n.= 2) SC-DARIC33 and CD19 CAR T cells using designs and manufacturing methods previously deployed in clinical trials at Seattle Children's Hospital. In these trials, CD19 CAR T cell administration resulted in complete remission rates of >90% in children and young adults with R/R B-cell malignancies (34, 35). Compared to control CD19 CAR T cell products, SC-DARIC33 showed similar expansion kinetics, CD4/CD8 ratios, proportions of CAR/DARIC+ cells and CAR/DARIC cell yields (**Fig. 5A**). The frequency of cells expressing both CD62L+ and CD45RO+, a phenotype associated with preserved engraftment fitness and antitumor potential(36), was >90% within each of the UTD, CD19 CAR, and SC-DARIC33 T cell products (**Fig. 5B**).

Previous preclinical studies performed by our group found control of Raji xenograft tumor burden progression correlated with clinical activity of CD19 CAR T cell designs (37).To compare anti-tumor activity across CD19- and CD33-targeted T cell therapies, we generated Raji cells with matched levels of CD19 and CD33 expression via lentiviral transduction (Raji.CD33.ff/luc). Progression of intravenously injected Raji.CD33.ff/luc xenograft tumor burden was monitored following administration of CD19 CAR, SC-DARIC33 (tested at two doses), and CD19-specific DARIC T cell products manufactured using a GMP process (see **Fig. 5C** for schema). As expected, no Raji tumor burden progression was observed following infusion of 1 x 10^7 CD19 CAR T cells per animal, whereas mice receiving no treatment, or rapamycin alone (0.1mg/kg qMWF delivered by intraperitoneal injection) showed rapid tumor growth and developed tumor-associated symptoms requiring euthanasia within 12 days (**Fig. 5D**). Infusion of either 3 x 10^7 or 1 x 10^7 SC-DARIC33 T cells followed by rapamycin dosing suppressed tumor growth and prolonged survival of mice compared to control animals not receiving rapamycin (**Fig. 5E**, $p = 0.028$ and $p = 0.004$). Administration of CD19-specific DARIC cells also resulted in rapamycin-dependent tumor suppression and prolonged survival in the Raji xenograft tumor model. Together, these data suggest SC-DARIC33 may require higher T cell doses to achieve similar potency as CD19 CAR T cells.

DARIC33 and SC-DARIC33 T cells display recursive rapamycin-dependent ON-OFF-ON functional state transitions.

The capacity to temporarily pause DARIC T cell effector function in patients following SC-DARIC33 administration represents a potential control feature for mitigating potential toxicities and permitting hematopoietic recovery. Moreover, therapeutic T cells that are intermittently rested may be less prone to functional exhaustion and capable of repopulating memory cell

compartments (29). We therefore developed systems to probe pharmacologic control of DARIC33 T cells. Kinetic assessments of DARIC33-induced cancer cell cytotoxicity showed rapid and complete rapamycin-dependent cancer cell killing only when the target antigen CD33 is expressed in cancer cells (**Fig. S7A,B**). Killing rates increased immediately following rapamycin addition, and was maximal after 37 hours (**Fig. S7C,D**). To define kinetic effects of rapamycin removal, DARIC33 T cells cultured with rapamycin for 24 hours were washed and rested for increasing periods of time in rapamycin-free media prior to challenge with CD33+ MV4-11 AML target cells. At early time points, pre-activated SC-DARIC33 T cells showed high levels of IFNγ release. Increasing durations of rest resulted in a progressive decline of IFNγ release that returned to baseline after 96 hours, following first-order kinetics characterized by a half-life of 17 hours (**Fig. 6A**).

To evaluate the reversibility of SC-DARIC33 T cell activation in vivo, we treated mice bearing AML xenografts derived from MV4-11 cells modified for BLI with SC-DARIC33 T cells and rapamycin delivered following continuous (Days 1-150), interrupted (Days 1-14 and 28 – 150), or abbreviated (Days 1-14) schedules (see **Fig. 6B** for schema). Mice receiving UTD control cells (with or without rapamycin) exhibited tumor growth and tumor associated symptoms by day 50, whereas mice treated with SC-DARIC33 T cells and rapamycin exhibited delayed tumor burden progression (**Fig. 6C**), and prolonged symptom-free survival (**Fig. 6F**). Four of 5 mice receiving the abbreviated rapamycin schedule exhibited tumor relapses approximately 21 days after rapamycin was discontinued. In contrast, when rapamycin was reinitiated on Day 28, 4 of 5 mice controlled the tumor through the end of the observation period. Estimates of tumor growth kinetics, modeled using linear mixed effects, revealed similar tumor growth rates in negative control groups and animals treated with SC-DARIC33 and abbreviated

rapamycin (**Fig. 6D, E**). However, among animal receiving either continuous or intermittent rapamycin, SC-DARIC33 T cells suppressed tumor growth rates and extended survival (**Fig. 6F**). Together, these data are consistent with a model wherein discontinuation of rapamycin pauses SC-DARIC33 anti-tumor activity, which may be restored by resuming rapamycin administration.

Preclinical models define blood rapamycin concentrations associated with SC-DARIC33 activation *in vitro* and *in vivo*.

To support rapamycin dose selection for first-in-human testing of SC-DARIC33, we sought to define rapamycin concentrations required for DARIC33 activation both *in vitro* and in a mouse xenograft tumor model. We used Förster Resonance Energy Transfer (FRET) to characterize the dimerization kinetics of the DARIC33 system *in vitro*. A PE-labeled anti-V_HH antibody was used as a donor fluorophore while an AlexaFluor 647-labeled anti-FRB antibody was used as an acceptor **(Fig. S8B)**. Labeling of DARIC33 cells with both antibodies, but not with either antibody alone, resulted in rapamycin-dependent fluorescence emission signal in the PE-Cy5 channel (**Fig S8A**), indicating heterodimer-dependent FRET. We quantified rapamycin-mediated dimerization parameters by culturing DARIC33 cells in a gradient of rapamycin concentrations in media and determined the rapamycin EC_{50} for DARIC33 dimerization was 135pM in T cell media (**Fig S8C**). To determine the time between rapamycin dosing and peak DARIC33 activation, we cultured DARIC33 T cells in rapamycin and analyzed the FRET signal at selected times after administration. The FRET signal, reflecting the combined effects of surface expression and dimerization, peaked at 8 hours post rapamycin addition, suggesting that DARIC33 activation is time dependent and reaches maximal levels soon after rapamycin addition (**Fig S8D**).

In patients, rapamycin is highly sequestered by erythrocytes due to highly abundant cytoplasmic FKBP-related proteins (38) and is bound to plasma proteins (39, 40) which both act to reduce the amount of unbound rapamycin available to bind to DARIC33. We therefore sought to understand the rapamycin concentrations required for DARIC33 heterodimerization and DARIC33 T cell activation in the presence of anticoagulated whole blood using both a FRET-based dimerization assay and an AML-stimulated cytokine release assay, respectively. Similar to T cell media (**Fig. S8C**), DARIC33 T cells cultured in whole blood exhibited a rapamycin-dependent increase in FRET signal (EC_{50}=11.4nM, **Fig. S8E**). Next, we performed overnight co-cultures of $CD33^{+}$ MV4-11 cells and DARIC33 T cells in either T cell culture media, human, or mouse whole blood samples. The DARIC33 samples exhibited rapamycin-dependent increases in IFNγ release that were similar in either species (IFNγ release, human blood, EC_{50} = 2.6 nM while mouse blood EC_{50} = 2.8 nM, **Fig. 7A**) and among human T cell donors (EC_{50} range of 1.5 nM – 6.3 nM across three T cell donors and two blood donors, examined in duplicate, n = 12 total). The T cell activation assays and FRET dimerization assays showed higher concentrations of rapamycin (~20-fold and ~100-fold, respectively) are required for half-maximal DARIC33 activity in whole blood as compared to media. These data define a target range of whole blood rapamycin concentrations capable of activating DARIC33 T cells in the presence of CD33-expressing tumor cells.

We next measured rapamycin exposure following single and repeat intraperitoneal (IP) administrations in tumor-bearing mice using a quantitative whole blood assay. Blood concentrations of rapamycin were generally dose proportional, peaking within 2 hours of administration and decaying with an elimination half-time between 16 and 24 hours (**Fig. 7B**).

Peak rapamycin concentrations ranged from 10 ng/mL at doses of 0.02mg/kg to near 100 ng/mL at a dose of 0.1 mg/kg (**Supplemental Table S2**).

To determine the impact of various rapamycin dose levels and dosing schedules on the anti-tumor activity of SC-DARIC33 T cells, we treated MV4-11 tumor bearing mice with SC-DARIC33 T cells followed by different rapamycin dosing and administration schedules (see **Fig. 7C** and **Fig. S9A** for detailed schema). Among mice receiving dosing regimens predicted to be inactive (e.g. rapamycin alone, UTD T cells with or without rapamycin, or SC-DARIC33 cells alone) tumor growth was similar compared to mice receiving no treatment (log[Flux]/day = –.26 - 0.27, **Fig. 7D-E**). In contrast, treatments predicted to be active (e.g., SC-DARIC33 product followed by rapamycin) exhibited lower rates of tumor growth, with the lowest rate observed among mice receiving 0.01mg/kg rapamycin IP daily (log[Flux]/day = 0.058). Tumor growth rates correlated with survival: while control mice developed tumor-associated symptoms near day 45, none of the mice receiving active treatment (DARIC33 + rapamycin) exhibited signs of tumor progression at this time point. All rapamycin doses tested prolonged survival ($p < 0.001$ log rank test): at the end of the 90-day observation period, treatment with SC-DARIC33 and 0.01mg/kg rapamycin daily continued to control tumor outgrowth in 5 of 10 mice (**Fig. S9B**).

Interestingly, while *in vitro* mouse and human whole blood assays showed similar rapamycin-dependent DARIC33 activation (**Fig. 7A**), we identified species differences in rapamycin red blood cell (RBC) partitioning and plasma protein binding (PPB) (**Table S3-4**). In humans, 94.5% of rapamycin is bound to RBCs while only 3.1% is found in plasma (39). In human plasma, rapamycin is highly protein bound (92%). In contrast, in mice we observed that rapamycin has 5.5% RBC partitioning and is greater than 99% PPB (**Table S5**). Despite these species-specific differences in rapamycin distribution in blood compartments, we observed

similar rapamycin EC50's for DARIC33 T cell activation in the presence of human or mouse whole blood (**Fig. 7A**), indicating that unbound rapamycin available to interact with DARIC33 was similar, and suggests this may also occur *in vivo*. Taken together, these data support DARIC33 activity across a wide range of rapamycin dosing in vivo and inform a target rapamycin trough (C_{24h}) blood concentration range of 1.5-3 ng/mL for DARIC33 T cell activation in humans.

First in human clinical experience demonstrates feasibility of rapamycin activation of SC-DARIC33

We designed PLAT08 (NCT05105152), as a first-in-human phase 1 trial evaluating the safety of escalating doses of SC-DARIC33 in pediatric and young adult patients with relapsed and refractory AML **(Fig. 8A)**. In this trial, subjects receive lymphodepleting chemotherapy followed by SC-DARIC33 T cell products and rapamycin. To identify rapamycin doses and schedules that maximize the likelihood of achieving rapamycin blood concentrations troughs within the target range of 1.5-4 ng/mL, we simulated rapamycin dose/exposure relationships from adult and pediatric patients by using population pharmacokinetic models(38, 41) and sampled anthropomorphic measurements for children (**Fig. S10A-B**). Among evaluated dosing schedules (**Fig. S10C-H**), rapamycin daily dosing of 0.50 mg/ m2 (for patients ≤1.5 m2) or 0.75 mg (for patients >1.5 m2) 0.5mg/m^2 is predicted to achieve target rapamycin trough concentrations of above 1.5 ng/mL, and peak concentrations below 8ng/mL in 90% of the pediatric population (**Fig. 8B**). The mean population rapamycin peak and trough (C_{24h}) levels are predicted to be between 2ng/mL and 4ng/mL, well below the range of rapamycin typically used for immunosuppression in solid organ transplant recipients (12-24ng/mL, (42)). We therefore selected the dose schedule of daily oral rapamycin at 0.5mg/m^2 for initial evaluation in pediatric patients.

To evaluate whether rapamycin exposure is associated with evidence of SC-DARIC33 tumor reactivity in patients, we evaluated infusion products and blood samples obtained from the first three patients enrolled on PLAT08 and treated at dose level 1 (DL1 = 10^6 DARIC$^+$ cells per kg). Infusion products contained between 49% and 57.9% DARIC$^+$ T cells (defined as those expressing surface V_HH). We developed a high dimensional flow cytometry panel capable of simultaneously evaluating markers of myeloid and T cell identity (CD33, CD3, CD4, and CD8), lentiviral transduction (V_HH and FRB), and T cell activation state (CD101, PD-1, and 4-1BB) in patient samples. We found similar proportions of DARIC$^+$ and DARIC$^-$ populations of CD8 T cells expressed activation markers following incubation of patient infusion products in media alone or media supplemented with rapamycin, demonstrating that exposure to rapamycin alone was insufficient to stimulate T cell activation (**Fig. 8D**). Using continuous rapamycin monitoring and dose adjustment, rapamycin concentrations in blood samples among the three subjects (S001, S002 and S004) were within the target range in 0/2 timepoints, 8/15 timepoints, and 14/18 timepoints, respectively (**Fig. 8E**). Finally, we monitored temporal trends in serum levels of a broad panel of cytokines enriched for analytes associated CAR T cell activation(34, 35) and successful CAR T cell therapy of lymphocytic leukemia (43). Serum samples from patient S004, which had the highest proportion of rapamycin concentration in blood falling within the target range, exhibited dramatic increases in IFNγ, TNFα and IL-6, peaking around day 10 post CAR infusion, followed by steady declines (**Fig. 8F**). These initial observations indicate that successfully achieving the target rapamycin concentration is associated with elevated levels of cytokines affiliated with CAR T cell activation.

Following observations that rapamycin stabilized surface FRB on DARIC33 cells (**Fig. 1E**), we hypothesized that FRB expression would correlate with rapamycin exposure. As expected,

evaluation of healthy donor T cell products using our clinical flow cytometry panel showed overnight exposure to rapamycin resulted in increased V_HH and FRB expression (**Fig. 9A**). Patient S002 exhibited chloromas, some of which developed increased hemorrhagic necrosis following SC-DARIC33 and rapamycin administration **(Fig. 9B)**. Flow cytometric evaluation of chloroma and peripheral blood tissue demonstrated preferential accumulation of VHH^+FRB^+ cells within the chloroma tissue (**Fig. 9C**). These cells had an activated phenotype, as the proportion of $PD1^+$ and $TIM3^+$ cells was higher among the VHH^+FRB^+ CD8 T cells compared to VHH^- ($DARIC33^-$) CD8 T cells (**Fig. 9D**). We next analyzed T cell expansion and functionality in patient S004. Among peripheral blood samples from patient S004, the proportion of circulating blast-like $CD33^{hi}$ side scatter (SSC^{low}) cells decreased by 99.8%, from 88% to 0.23% from day 7 to day 15 (**Fig. 9E**). This was accompanied by concurrent expansion of $DARIC33^+$ T cells within the peripheral blood, peaking at 6% of total lymphocytes and 20.5% of circulating T cells on day 9 post CAR infusion, before contracting (**Fig. 9F**). Evaluation of surface phenotypes of $V_HH^+FRB^+$ ('RAPA exposed') CD8 T cells showed progressively increasing expression of activation markers, including PD-1, TIM3 and 4-1BB, within RAPA exposed CD8+ T cells from days 9 through 21 (**Fig. 9G**). In contrast, DARIC33-negative CD8 T cells presented with a transient increase in surface TIM3 and PD-1 at day 15 that was not sustained. These data show that, in the presence of tumor antigen and rapamycin, SC-DARIC33 expands, engrafts, and acquires activated states. SC-DARIC33 activation and expansion was temporally coincident with increases cytokine markers of T cell activation and transient depletion of $CD33^{hi}$ cells in peripheral blood. Together, these findings provide initial in human evidence that the DARIC33 platform achieves rapamycin responsive antigen dependent T cell activation.

DISCUSSION

In this report we describe preclinical characterization and first clinical data from a distinct CAR T cell platform that aims to solve difficult challenges in treating AML through a drug regulated DARIC architecture. Targeting AML with CAR T cells presents specific challenges, as overlapping expression of target antigens on myeloid cells and hematopoietic stem cells limits the therapeutic window for constitutively active CARs. Here, we describe the development of a regulated anti-AML CAR T cell therapy that targets a membrane proximal domain CD33 epitope. Rapamycin-dependent heterodimerization of DARIC components results in a stringent OFF state in the absence of rapamycin and acquisition of an effector ON-state T cell in the presence of low nanomolar rapamycin concentrations. As a benchmark, we compared DARIC33 T cells to a CD19 CAR production design that has achieved clinical efficacy (34, 35). The two architectures demonstrate similar potency *in vitro* and comparable potency in challenging *in vivo* models. The DARIC33 system, composed exclusively of human or humanized domains, and using clinically tolerable dosing of a FDA approved drug (rapamycin), represents a substantial advance over other regulated CAR formats. We have initiated clinical testing of the DARIC33 system and observed endpoints consistent with T cell activation, expansion, and early signs of anti-tumor activity.

Precise control of CAR T cell activity may help mitigate toxicities associated with CAR T engraftment syndromes such as cytokine storm and/or the aplasia that occurs from targeting a cell lineage specific antigen such as CD19 and CD33. Following infusion, CAR T cells can proliferate dramatically after synchronous activation by abundant tumor cells or their antigen expressing non-malignant counterparts and release of effector cytokines resulting in potentially fatal cytokine release syndrome and neurotoxicity (2, 44). These adverse effects limit CAR

dosing but could potentially be mitigated by pausing CAR activity such that DARIC products infused in the OFF-state may be subject to pulses of rapamycin induction to drive engraftment and incrementally reduce tumor burden. While the risks of B-cell aplasia following CD19 CAR T cell therapy may be mitigated by immunoglobulin infusions, indefinite elimination of cells expressing AML associated antigens such as CD33, CD123, CLL1/CLEC12A, or CD38 is likely to result in clinically intolerable myelosuppression. Thus, when treating AML, strategies to mitigate hematopoietic toxicity are likely to be a requirement.

Individualizing OFF-state ON-state sequencing may tailor therapeutic windows to patient-specific circumstances (45) and represents a useful feature of the DARIC platform. Intermittent cycling of DARIC33 activity through metronomic rapamycin dosing may enable episodic hematopoietic recovery between cycles of active leukemic targeting. While the half-life of rapamycin precludes rapid cessation of DARIC T cell function, pharmacologic inhibitors of proximal antigen receptor signaling, such as dasatinib (46, 47), in combination with rapamycin withdrawal may represent an alternative strategy for managing acute toxicities arising from unrestrained T cell activation. In addition, periods of alternating signaling and quiescence may enhance the efficacy of anti-tumor T cells by preventing T cell exhaustion(48–50) and allowing effector T cells to transition to memory states(29, 30, 51–54) after periods of prolonged antigen exposure. We are currently evaluating transcriptional and epigenetic changes in SC-DARIC33 cells following rapamycin interval dosing to analyze the impact of paused T cell activity on T cell memory state transitions. Temporal pauses of CAR activity may therefore be a general method to promote or sustain the fitness of engineered therapeutic T cells.

Controllable CAR designs may open new paradigms of CAR T cell therapy that directly address both prevailing failure mechanisms and risks to patients. For example, controllable CAR

T cells may allow administration of higher cell doses followed by individualized titration of the activating drugs, widening therapeutic windows (45). In addition, whereas constitutive potency enhanced CARs risk runaway reactivity that may be difficult to bring back under control (55, 56), regulated CAR designs may promote the safety of genetic potency enhancement strategies that attempt to further CAR T cell survival, expansion or reactivity. Finally, if intermittent T cell activation leads to a formation of a long-lived DARIC T cell niche, patients could be re-dosed with rapamycin to control any tumor recurrence following the initial remission. Overall, clinical validation of a controllable CAR T cell designs will impact multiple research questions and clinical outcomes within the cellular therapy field. The on-going first-in-human trial of SC-DARIC33 for children and young adults with relapsed or refractory CD33+ AML will provide clinical and corelative data supporting the pharmacologic control of CAR T products, as well as AML- and myeloid cell- targeting attributes of this next-generation cellular therapeutic.

MATERIALS AND METHODS

Sex as a biological variant

Murine xenograft studies used female mice to minimize size variation. Results are expected to be relevant to all humans.

Cell Lines

Cell lines were obtained from the following sources: MOLM-14 (ACC 777), and MV4-11 (ACC 102) were purchased from DSMZ; A549 (CCL-185) and THP1 (TIB-202) were purchased from ATCC; HL-60 was provided by the Bhatia lab (Fred Hutchinson Cancer Research Center, Seattle, WA, USA). HL60, MV4-11 and MOLM14 were engineered to express GFP and firefly luciferase via lentiviral transduction. GFP+ cells were FACS sorted to generate uniformly positive cell population. Raji cells engineered to express GFP and firefly luciferase were further modified to express CD33M (NM_001772) by lentiviral transduction, followed by FACS sorting and limiting dilution cloning to select expression of equivalent CD19 and CD33 antigen concentrations. K562 was transduced with lentivirus to express membrane bound OKT3 as a positive control for in vitro T cell activity assays. HL-60, MOLM14, MV4-11, THP1 cells were cultured in RPMI-1640 supplemented with 10% FBS and 1% L-glutamine, referred to as complete RPMI.

CD33-Targeted DARIC-V_HH Lentiviral Vector Design and Production

DARIC lentiviral vectors were generated as previously described(4). Briefly, transgenes encoding the CD33-specific V_HH binders were synthesized incorporating sequence modifications that optimized codon usage and enhanced human immune tolerance and cloned into the

previously described CD19-DARIC transfer plasmid (4) using Gibson cloning (NEB). Cloned products were verified using Sanger sequencing.

A four-plasmid self-inactivating lentiviral production system was used. Briefly, the DARIC transfer vectors mixed with envelope and packaging vectors were transfected into 293T cells using TransIt transfection reagent (Mirus Bio). Vector-containing supernatant was collected, passed through a 0.2 micron filter and either used immediately or stored at -80 until use. In some cases, vector supernatant was concentrated by centrifugation at 10,000*g* x 4 hours prior to cryopreservation. Analysis of Virus Copy Number (VCN) was performed as described previously (4).

DARIC T Cell Manufacture

Thawed PBMCs were resuspended in TCGM supplemented with 250 IU/ml recombinant human IL-2 (Stemcell, catalog 78220.3) prior to activation with 50ng/ml anti-CD3 (clone OKT3) and anti-CD28 (clone 15E8) antibodies (Miltenyi Biotec). Lentivirus supernatants were added to PBMC cultures 24 hours later (multiplicity of infection [MOI] = 10). 72 hours after activation, transduced PBMC were collected, washed, and resuspended in complete TCGM with human IL-2 at 0.5 x 10^6 cells/ml and transferred to gas permeable culture vessels (G-REX, WilsonWolf). PBMC cultures were expanded in vitro at cell density of 0.5-2 x 10^6 cells/ml maintained by the addition of fresh media every 2-3 days for a total of 10-11 days until cryopreservation. Clinical T cell product manufacture was completed as essentially as described (57), except T cell cultures were initiated with a 1:1 ratio of CD4 and CD8 T cells.

Cytokine Release Assay

For cytokine production analysis, 0.1×10^6 T cells were cocultured with 5×10^4 target cells (effector:target ratio = 2:1) for 24 hours with or without rapamycin (1 nM, unless otherwise specified) in TCGM. Culture supernatants were evaluated using the V-PLEX Proinflammatory Panel 1 Human kit (Meso Scale Diagnostic) and analyzed by the MESO QuickPlex SQ 120 Instrument (Meso Scale Diagnostic) according to the manufacturer's instructions.

Murine Xenograft Models

Female adult (8-12 week-old) NOD/Scid IL-2RC^{null}(NSG) mice were bred in house or purchased from the Jackson Laboratory (Bar Harbor, ME) and housed in specific pathogen free conditions with as 12-hour light/dark cycle and monitored daily by veterinary staff or research scientists. All experiments were carried out following Institutional Animal Care and Use Committee (IACUC) approved protocols. Mice exhibiting hunched posture, decreased mobility that impaired feeding, single or multiple tumors totaling >1cm in diameter, >20% weight loss or loss of skin integrity were humanely euthanized. Development of tumor associated symptoms requiring euthanasia was considered an event for the purposes of Kaplan Meier analyses.

Cultures of tumor cells modified for bioluminescence imaging (BLI) were washed and resuspended in phosphate buffered saline (PBS). Cell densities were adjusted to contain the following cell doses within 200uL as follows: HL60 (5×10^6), MV4-11 (1×10^6), MOLM14 (1×10^5), or Raji (0.5×10^6). Tumor cell suspensions were administered via lateral tail vein injection.

BLI was performed by intraperitoneal or subcutaneous injection of 4.29mg per mouse of D-luciferin (Xenogen) at various timepoints prior to and after tumor inoculation. Prior to treatment, mice were distributed so that treatment groups had similar median bioluminescence. Mice

exhibiting tumor signal only within the tail were excluded from studies. Imaging of isoflurane anesthetized mice occurred 15min after D-luciferin injection using the IVIS Spectrum Imaging System (PerkinElmer). Luciferase activity was analyzed using Living Image Software version 4.5.2 (PerkinElmer).

Prior to administration to recipient mice, cryopreserved T cell products were thawed into human AB serum, washed with PBS, counted, and resuspended in PBS such that a single dose of T cells was administered in a total volume of 200uL. Cells suspensions were maintained on ice until injection via the lateral tail vein of recipient mice. Mice received a single injection of cells. To determine cell dosing, the total number of DARIC33 T cells and CD19 DARIC T cells administered to mice were calculated on the basis of FRB+ cells, i.e. *total cells = desired cell dose* / (*proportion FRB+*). Similarly, the total number of CD19 CAR T cell products were determined on the basis of the proportion of cells expressing the EGFRt marker(58). The total cell dose of untransduced (UTD) control T cell products was matched to highest total number of T cells administered within a given experiment.

Mice assigned to rapamycin treatment received rapamycin by intraperitoneal injection either daily or every Monday, Wednesday, and Friday as specified within schemas and/or figure legends. Solutions of rapamycin for injection were prepared by dilution of a 10mM DMSO stock into PBS immediately prior to administration such that final concentration of DMSO was < 0.2% (v/v). For weight-based dosing, mouse weights were determined weekly and used to adjust rapamycin dosing. The total volume of rapamycin solution administered ranged from 50uL to 200uL.

Statistical Analysis

Statistical significance was determined by a P value of < 0.05 using GraphPad Prism 9 software or the lme4 package of the R statistical computing package. Tumor symptom free survival of mice within studies were compared using Kaplan Meier method and the log rank test. Global comparisons for studies with more than 2 groups were conducted, and if significant, pairwise comparisons were examined using a false discovery rate of 0.05. Logistic dose response curves were evaluated in GraphPad Prism 9.

Evaluation of blood, serum and chloroma samples from patients

PLAT08 is an ongoing phase 1 study of $CD4^+$ and $CD8^+$ T cells lentivirally transduced to express the DARIC33 transgene, delivered via intravenous infusion following lymphodepleting chemotherapy in pediatric and young adult patients (<30 years old) with relapsed or refractory acute myeloid leukemia (NCT050105152). The study is conducted in accordance with FDA and international conference on harmonization guidelines for good clinical practice, the declaration of Helsinki and applicable institutional review board guidelines (study protocol approved by Seattle Children's Institutional Review Board). All patients or their guardians provided written informed consent for trial participation. Written informed consent was received for the use of photographs and the record of informed consent has been retained at Seattle Children's. Following enrollment, $CD4^+$ and $CD8^+$ T cells isolated from cells collected by leukopheresis were combined in a 1:1 ratio to manufacture SC-DARIC33 as described (57). Freshly obtained blood, marrow, or chloroma samples from patients following SC-DARIC33 infusion were evaluated by immunophenotyping following RBC lysis using standard staining and flow cytometry techniques (see Supplementary Methods for additional details).

Data and materials availability

Requests for materials will be fulfilled following requests to corresponding authors and completion of appropriate material transfer agreements. High throughput sequencing data (RNAseq) has been deposited in the Genome Expression Omnibus at NCBI, accession #GSE255002. Code used to evaluate CD33 splicing from sequence read archives will be made available following request to A.A. Supporting Data Values associated with each figure is provided in a supplemental spreadsheet.

See *supplementary materials* for additional study details and descriptions.

List of Supplementary Materials

Supporting Data Values

Supplemental Materials and Methods

Fig S1 to S10

Table S1 to S5

References

1. Ghorashian S, et al. Enhanced CAR T cell expansion and prolonged persistence in pediatric patients with ALL treated with a low-affinity CD19 CAR. *Nat Med*. 2019;25(9):1408–1414.

2. Juluri KR, et al. Severe cytokine release syndrome is associated with hematologic toxicity following CD19 CAR T-cell therapy. *Blood Adv*. 2022;6(7):2055–2068.

3. Perna F, et al. Integrating Proteomics and Transcriptomics for Systematic Combinatorial Chimeric Antigen Receptor Therapy of AML. *Cancer Cell*. 2017;32(4):506-519.e5.

4. Leung W-H, et al. Sensitive and adaptable pharmacological control of CAR T cells through extracellular receptor dimerization. *JCI Insight*. 2019;4(11). https://doi.org/10.1172/jci.insight.124430.

5. Wu C-Y, et al. Remote control of therapeutic T cells through a small molecule–gated chimeric receptor. *Science*. 2015;350(6258):aab4077.

6. Mahalati K, Kahan BD. Clinical Pharmacokinetics of Sirolimus. *Clin Pharmacokinet*. 2001;40(8):573–585.

7. Walter RB, et al. Acute myeloid leukemia stem cells and CD33-targeted immunotherapy. *Blood*. 2012;119(26):6198–6208.

8. Pérez-Oliva AB, et al. Epitope mapping, expression and post-translational modifications of two isoforms of CD33 (CD33M and CD33m) on lymphoid and myeloid human cells. *Glycobiology*. 2011;21(6):757–770.

9. Stankunas K, Crabtree GR. Exploiting protein destruction for constructive use. *Proc Natl Acad Sci*. 2007;104(28):11511–11512.

10. Edwards SR, Wandless TJ. The Rapamycin-binding Domain of the Protein Kinase Mammalian Target of Rapamycin Is a Destabilizing Domain*. *J Biol Chem*. 2007;282(18):13395–13401.

11. Schreiber KH, et al. A novel rapamycin analog is highly selective for mTORC1 in vivo. *Nat Commun*. 2019;10(1):3194.

12. Lamba JK, et al. CD33 splicing SNP regulates expression levels of CD33 in normal regenerating monocytes in AML patients. *Leuk Lymphoma*. 2018;0(0):1–4.

13. Laszlo GS, et al. Expression and functional characterization of CD33 transcript variants in human acute myeloid leukemia. *Oncotarget*. 2016;7(28):43281–43294.

14. Mortland L, et al. Clinical Significance of CD33 Nonsynonymous Single-Nucleotide Polymorphisms in Pediatric Patients with Acute Myeloid Leukemia Treated with Gemtuzumab-Ozogamicin–Containing Chemotherapy. *Clin Cancer Res*. 2013;19(6):1620–1627.

15. Malik M, et al. CD33 Alzheimer's Risk-Altering Polymorphism, CD33 Expression, and Exon 2 Splicing. *J Neurosci*. 2013;33(33):13320–13325.

16. Raj T, et al. CD33: increased inclusion of exon 2 implicates the Ig V-set domain in Alzheimer's disease susceptibility. *Hum Mol Genet*. 2014;23(10):2729–2736.

17. Jetani H, et al. Siglec-6 is a novel target for CAR T-cell therapy in acute myeloid leukemia. *Blood*. 2021;138(19):1830–1842.

18. Gale RE, et al. No evidence that CD33 splicing SNP impacts the response to GO in younger adults with AML treated on UK MRC/NCRI trials. *Blood*. 2018;131(4):468–471.

19. Lamba JK, et al. CD33 Splicing Polymorphism Determines Gemtuzumab Ozogamicin Response in De Novo Acute Myeloid Leukemia: Report From Randomized Phase III Children's Oncology Group Trial AAML0531. *J Clin Oncol*. 2017;35(23):2674–2682.

20. Godwin CD, et al. Targeting the membrane-proximal C2-set domain of CD33 for improved CD33-directed immunotherapy. *Leukemia*. 2021;35(9):2496–2507.

21. Nair-Gupta P, et al. A novel C2 domain binding CD33xCD3 bispecific antibody with potent T-cell redirection activity against acute myeloid leukemia. *Blood Adv*. 2020;4(5):906–919.

22. Godwin CD, et al. The CD33 splice isoform lacking exon 2 as therapeutic target in human acute myeloid leukemia. *Leukemia*. 2020;34(9):2479–2483.

23. Brashem-Stein C, Andrews RG. Ontogeny of Hematopoietic Stem Cell Development: Reciprocal Expression of CD33 and a Novel Molecule by Maturing Myeloid and Erythroid Progenitors;8.

24. Knapp DJHF, et al. Single-cell analysis identifies a CD33+ subset of human cord blood cells with high regenerative potential. *Nat Cell Biol*. 2018;20(6):710–720.

25. Kenderian SS, et al. CD33-specific chimeric antigen receptor T cells exhibit potent preclinical activity against human acute myeloid leukemia. *Leukemia*. 2015;29(8):1637–1647.

26. Mardiana S, Gill S. CAR T Cells for Acute Myeloid Leukemia: State of the Art and Future Directions. *Front Oncol*. 2020;10. https://www.frontiersin.org/article/10.3389/fonc.2020.00697. Accessed May 16, 2022.

27. Schneider D, et al. A Unique Human Immunoglobulin Heavy Chain Variable Domain-Only CD33 CAR for the Treatment of Acute Myeloid Leukemia. *Front Oncol*. 2018;8. https://doi.org/10.3389/fonc.2018.00539.

28. Laborda E, et al. Development of A Chimeric Antigen Receptor Targeting C-Type Lectin-Like Molecule-1 for Human Acute Myeloid Leukemia. *Int J Mol Sci*. 2017;18(11):2259.

29. Weber EW, et al. Transient rest restores functionality in exhausted CAR-T cells through epigenetic remodeling. *Science*. [published online ahead of print: April 2, 2021]. https://doi.org/10.1126/science.aba1786.

30. Lynn RC, et al. c-Jun Overexpressing CAR-T Cells are Exhaustion-Resistant and Mediate Enhanced Antitumor Activity. *bioRxiv*. 2019;653725.

31. Anderson ND, et al. Transcriptional signatures associated with persisting CD19 CAR-T cells in children with leukemia. *Nat Med*. 2023;29(7):1700–1709.

32. Wilson TL, et al. Common Trajectories of Highly Effective CD19-Specific CAR T Cells Identified by Endogenous T-cell Receptor Lineages. *Cancer Discov*. 2022;12(9):2098–2119.

33. Good CR, et al. An NK-like CAR T cell transition in CAR T cell dysfunction. *Cell*. 2021;184(25):6081-6100.e26.

34. Gardner RA, et al. Intent to treat leukemia remission by CD19CAR T cells of defined formulation and dose in children and young adults. *Blood*. 2017;blood-2017-02-769208.

35. Finney OC, et al. CD19 CAR T cell product and disease attributes predict leukemia remission durability. *J Clin Invest*. 2019;129(5):2123–2132.

36. Wang X, et al. Comparison of naïve and central memory derived CD8+ effector cell engraftment fitness and function following adoptive transfer. *Oncoimmunology*. 2016;5(1):e1072671.

37. Summers C, et al. CD22 CAR Optimization for Improved in-Human Activity Following Inadequate CD22 CAR Activity in Phase 1 Clinical Trial PLAT-04. *Blood*. 2021;138(Supplement 1):403.

38. Wu K, et al. Nonlinear Population Pharmacokinetics of Sirolimus in Patients With Advanced Cancer. *CPT Pharmacomet Syst Pharmacol*. 2012;1(12):17.

39. Yatscoff R, et al. Blood distribution of rapamycin. *Transplantation*. 1993;56(5):1202–1206.

40. Trepanier DJ, et al. Rapamycin: distribution, pharmacokinetics and therapeutic range investigations: an update. *Clin Biochem*. 1998;31(5):345–351.

41. Goyal RK, et al. Sirolimus Pharmacokinetics in Early Postmyeloablative Pediatric Blood and Marrow Transplantation. *Biol Blood Marrow Transplant J Am Soc Blood Marrow Transplant*. 2013;19(4):569–575.

42. Sirolimus (Rapamune) FDA Label [Internet]. 2017. https://www.accessdata.fda.gov/drugsatfda_docs/label/2017/021083s059,021110s076lbl.pdf. Accessed May 2, 2022.

43. Hay KA, et al. Factors associated with durable EFS in adult B-cell ALL patients achieving MRD-negative CR after CD19 CAR T-cell therapy. *Blood*. 2019;133(15):1652–1663.

44. Acharya UH, et al. Management of cytokine release syndrome and neurotoxicity in chimeric antigen receptor (CAR) T cell therapy. *Expert Rev Hematol*. 2019;12(3):195–205.

45. Labanieh L, et al. Enhanced safety and efficacy of protease-regulated CAR-T cell receptors. *Cell*. 2022;185(10):1745-1763.e22.

46. Mestermann K, et al. The tyrosine kinase inhibitor dasatinib acts as a pharmacologic on/off switch for CAR T cells. *Sci Transl Med*. 2019;11(499). https://doi.org/10.1126/scitranslmed.aau5907.

47. Weber EW, et al. Pharmacologic control of CAR-T cell function using dasatinib. *Blood Adv*. 2019;3(5):711–717.

48. Singh N, et al. Impaired Death Receptor Signaling in Leukemia Causes Antigen-Independent Resistance by Inducing CAR T-cell Dysfunction. *Cancer Discov*. 2020;10(4):552–567.

49. Fraietta JA, et al. Determinants of response and resistance to CD19 chimeric antigen receptor (CAR) T cell therapy of chronic lymphocytic leukemia. *Nat Med*. 2018;24(5):563–571.

50. Zebley CC, et al. CD19-CAR T cells undergo exhaustion DNA methylation programming in patients with acute lymphoblastic leukemia. *Cell Rep*. 2021;37(9):110079.

51. Eyquem J, et al. Targeting a CAR to the TRAC locus with CRISPR/Cas9 enhances tumour rejection. *Nature*. 2017;543(7643):113–117.

817 52. Long AH, et al. 4-1BB costimulation ameliorates T cell exhaustion induced by tonic
818 signaling of chimeric antigen receptors. *Nat Med*. 2015;21(6):581–590.

819 53. Chen GM, et al. Integrative Bulk and Single-Cell Profiling of Premanufacture T-cell
820 Populations Reveals Factors Mediating Long-Term Persistence of CAR T-cell Therapy.
821 *Cancer Discov*. 2021;11(9):2186–2199.

822 54. Bai Z, et al. Single-cell multiomics dissection of basal and antigen-specific activation states
823 of CD19-targeted CAR T cells. *J Immunother Cancer*. 2021;9(5):e002328.

824 55. Narayan V, et al. PSMA-targeting TGFβ-insensitive armored CAR T cells in metastatic
825 castration-resistant prostate cancer: a phase 1 trial. *Nat Med*. 2022;28(4):724–734.

826 56. Krenciute G, et al. Transgenic Expression of IL15 Improves Antiglioma Activity of
827 IL13Rα2-CAR T Cells but Results in Antigen Loss Variants. *Cancer Immunol Res*.
828 2017;5(7):571–581.

829 57. Ceppi F, et al. Modified Manufacturing Process Modulates CD19CAR T-cell Engraftment
830 Fitness and Leukemia-Free Survival in Pediatric and Young Adult Subjects. *Cancer*
831 *Immunol Res*. 2022;10(7):856–870.

832 58. Wang X, et al. A transgene-encoded cell surface polypeptide for selection, in vivo tracking,
833 and ablation of engineered cells. *Blood*. 2011;118(5):1255–1263.

834

Acknowledgments: The authors thank Gracie Hoidal, James Rottman, Sumanti Sundaram and Rubina Corazzini for scientific discussions and expert technical assistance with the performance of in vivo studies, Aalton Lande for clinical scale research T cell product manufacturing assistance as well as the Therapeutic Cell Production Core for clinical infusion product manufacturing and methods development. We also thank the Correlative Sciences Lab for their assistance in research coordination and correlative sample processing. JSA is a recipient of the Paul Calabresi Career Development Award for Clinical Oncology K12-CA076930, the Translational Research Training in Hematology award from the American Society of Hematology (ASH) & The European Hematology Association, and the Scholar Award from ASH.

Author contributions:

Conceptualization: JSA, AEP, KO, GT, MF, JJ, MP, JAG, AA, MCJ

Methodology: JSA, AP, KO, GT, MF, MH, DEZ, SRR, NT, SH, MP, JAG, AA

Investigation: KO, JZ, WHL, UM, ARK, DX, PPLS, SKH, CE, SS, RL, PL, MF, RAC, SS, KJ, AS, WC, JT, AH, BE, SB, JW, SRR, NT

Visualization: JSA, AA, SRR, NT, DEZ

Funding acquisition: JSA, MCJ, JJ, PDG

Project administration: JSA, JJ, JAG, MCJ

Supervision: JSA, JJ, JAG, AA, MCJ

Writing – original draft: JSA, AA

Writing – review & editing: JSA, JJ, MP, PDG, JAG, AA, MCJ

Competing interests: WHL, AA, MP and JJ are holders of patents related to DARIC. MCJ is a holder of patents related to CD19 CAR T cells. AEP, JZ, WHL, DX, PPLS, SKH, UM,

ARK, DEZ, PL, PDG, JJ, MP and AA are current or former employees of 2seventy bio and own equity in 2seventy bio.

FIGURES

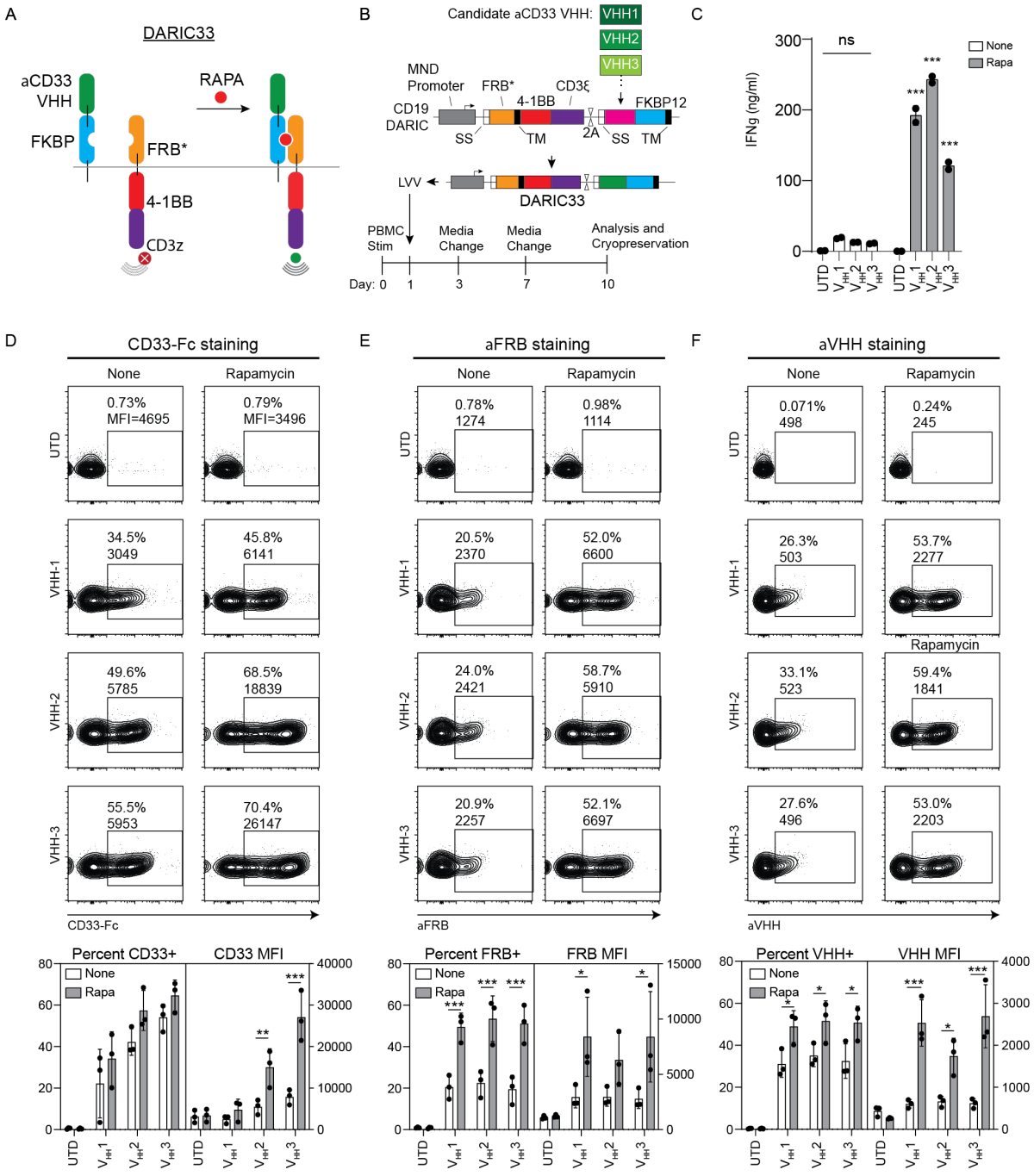

Figure 1. Rapamycin licenses antigen dependent DARIC33 T cell responses and stabilizes surface expression of DARIC33 components. (**A**) Schematic depicting rapamycin (rapa)

dependent activation of DARIC33. In the absence of rapa, the two DARIC components are split and do not respond to antigen. Following rapa addition, heterodimerization of DARIC components enables antigen dependent T cell responses. (**B**) Schematic depicting generation of DARIC33 candidates and T cell production. DNA sequences encoding modified VHH sequences are incorporated into DARIC33 lentiviral expression vectors. (**C**) IFNγ release by DARIC33 cell products following coculture with CD33+ MV4-11 AML cells. One of $n = 3$ donors shown. ****$p < 0.0001$, ANOVA with Tukey's multiple comparison correction. (**D-F**) Rapamycin stabilizes surface expression of DARIC33 components. DARIC33 cell products were cultured in media or media containing 1nM rapa overnight prior to staining and evaluation by flow cytometry. Representative flow cytometry plots from one of three donors (*above*) with quantitation of %pos and median fluorescence intensity from all three donors (*below*) *** $p < 0.001$, ** $p < 0.01$, * $p < 0.05$, 2-way ANOVA with Sidak's multiple comparison correction, $n = 3$ donors. (**D**) Rapa increases antigen binding capacity of DARIC33 cells. (**E**) Rapa increases surface expression of the antigen signaling arm of DARIC. (**F**) Rapa increases surface expression of the antigen recognition arm of DARIC.

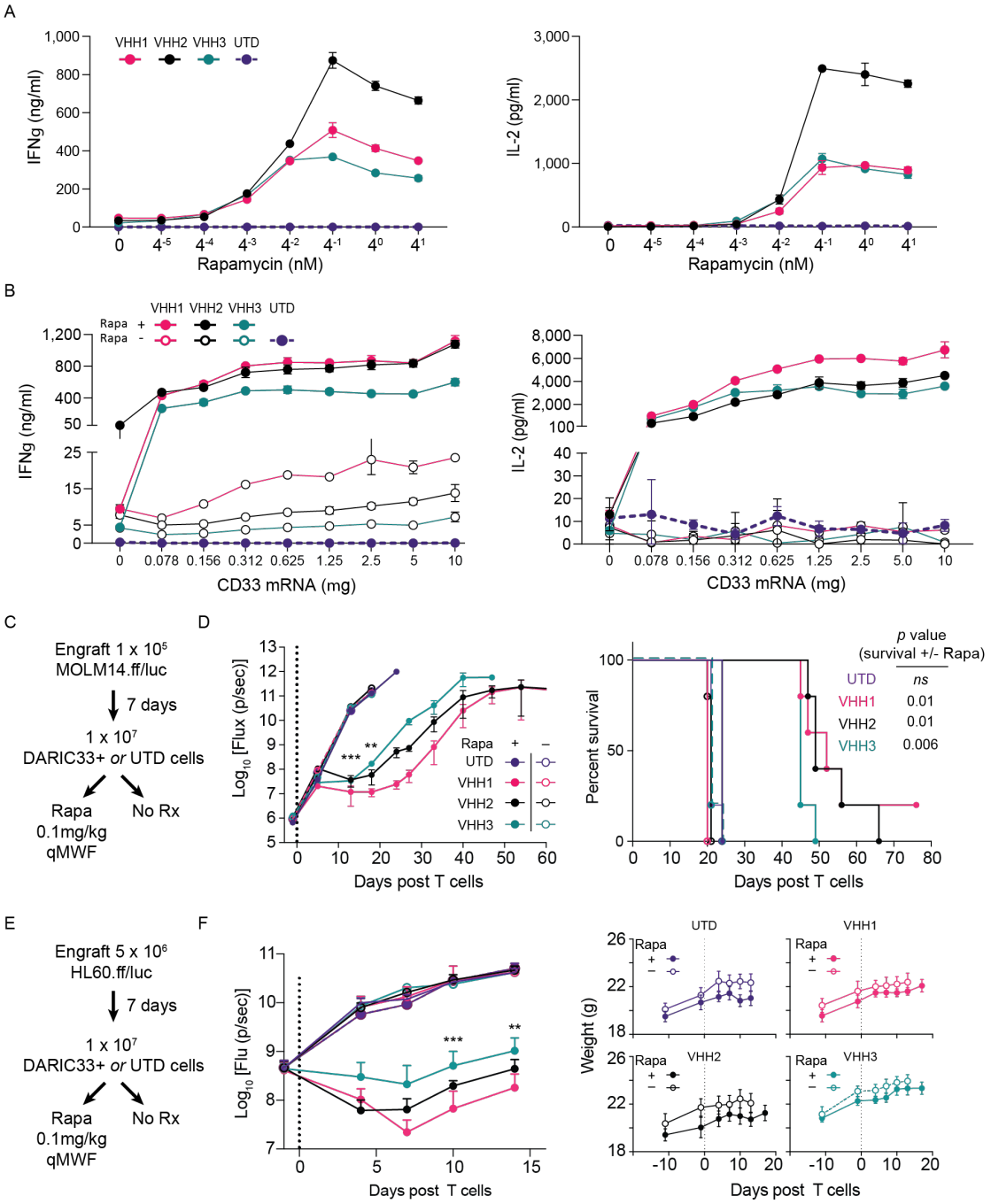

883

884 **Figure 2. DARIC33 stimulated T cell responses require low levels of target antigen and low**

885 **concentrations of rapamycin.** (**A**) Cytokine release by DARIC33 cells following coculture with

886 MV4-11 AML target cells in the presence of increasing concentrations of rapa. IFNγ is shown

887 *left*, IL2 is shown *right*. (**B**) Cytokine release by UTD (control) or DARIC33 cells following
888 coculture with or without rapa and HEK293 T cells electroporated with increases amounts of
889 CD33 mRNA. (**C-D**) 10^7 DARIC33+ cells, or an equivalent number of UTD control cells were
890 infused intravenously (IV) in NSG mice 7 days after engraftment of 1×10^5 MOLM14.ff/luc
891 leukemia cells per animal. Following T cell infusion, mice were treated 3 times per week with
892 0.1mg/kg rapamycin or were observed. (**D**) Quantification of tumor growth by BLI *left*; mean +
893 s.e.m., $n = 5$ mice per group (*left*) and symptom-free survival (*right*) with comparisons by
894 Mantel-Cox (Log-rank) test. (**E-F**) 10^7 DARIC33+ cells, or an equivalent number of UTD
895 control cells were infused intravenously (IV) in NSG mice 7 days after engraftment of 5×10^6
896 HL-60.ff/luc leukemia cells per animal. Following T cell infusion, mice were treated 3 times per
897 week with 0.1mg/kg rapamycin or were observed. (**F**) Quantification of tumor growth by BLI,
898 *left*, mean + s.e.m., n = 5 mice per group and mouse weight (right). Time points where all
899 DARIC33 formats meet the *p*-value threshold when compared to UTD cells + rapa (panels *D* and
900 *F*) are indicated as *** $p < 0.001$, ** $p < 0.01$, , using repeated measures ANOVA with
901 Dunnett's multiple comparison correction.
902

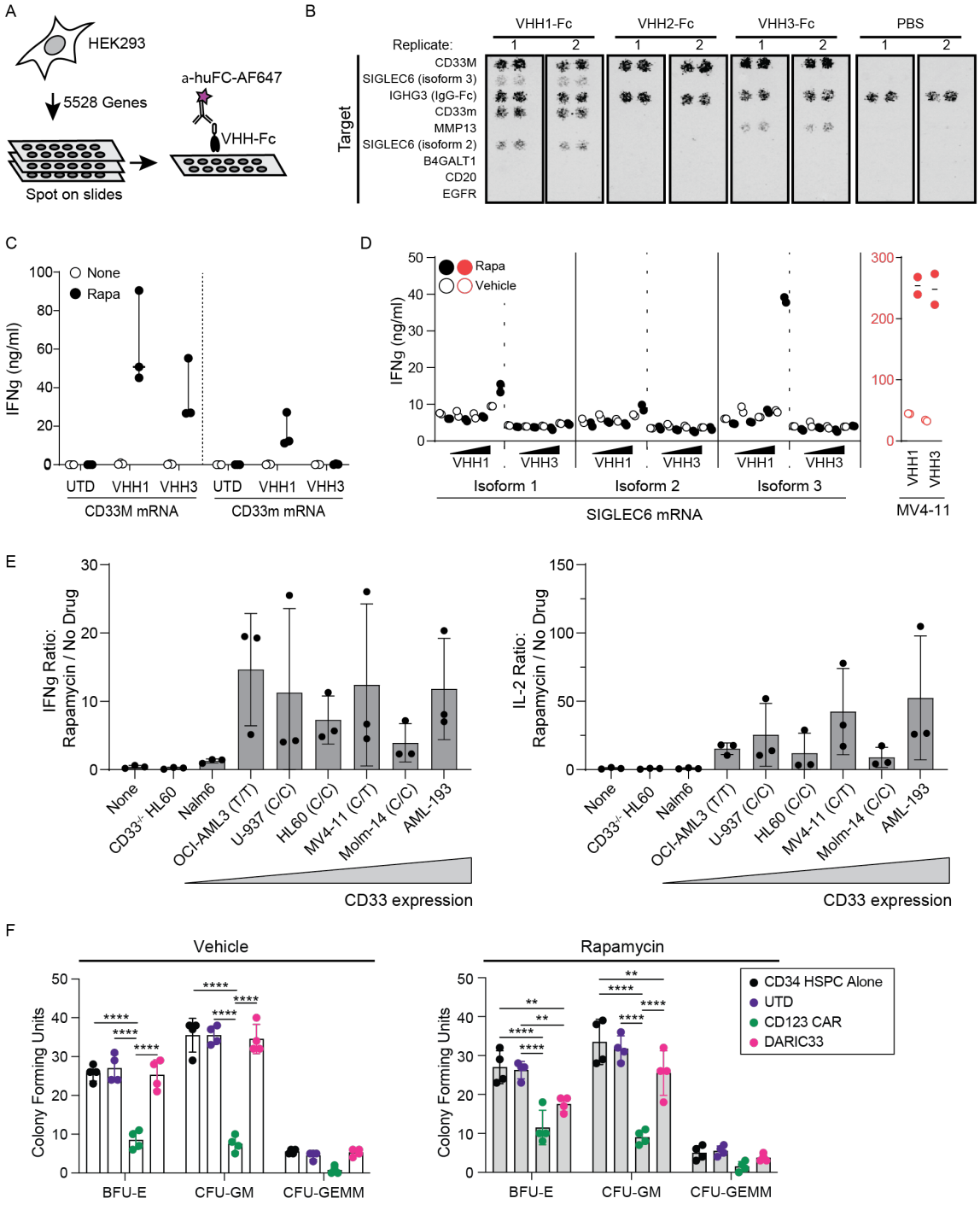

Figure 3. DARIC33 is specific for CD33 antigen and does not inhibit HSPC colony formation. (**A-B**) Evaluation of CD33-specific V_HH-Fc fusion proteins used in DARIC33 designs. (**A**) Schematic depicting detection strategy of V_HH-Fc fusions binding to HEK293 cells

907 expressing one of 5,528 surface-bound or secreted proteins. Following reverse transfection
908 HEK293 cells are spotted onto slides then stained with V_HH-Fc proteins (or PBS a control) and
909 alexa647-labeled anti-human-Fc secondary antibodies. (**B**) Secondary screen of selected hit and
910 control transgenic HEK293 samples (n = 2 replicates shown). (**C**) Stimulation of T cell IFNγ
911 release by DARIC33 designs in the presence of rapa following exposure to HEK293 cells
912 electroporated with mRNA encoding CD33M (*left*) and CD33m (*right*). (**D**) Stimulation of T cell
913 IFNγ release by DARIC33 designs in the presence of rapa following exposure to HEK293 cells
914 electroporated with mRNA encoding Siglec6 (*left*). Release of IFNγ following coculture of
915 DARIC33 with MV4-11 AML cells is shown for comparison (*right*). (**E**) Correlation of CD33
916 density (expressed as the logarithm of the antigen binding capacity) with release of IFNγ (*left*)
917 and IL-2 (*right*). (**F**) Colony forming units following culture of CD34+ cells alone or with T cells
918 in the presence or absence of rapa. Colonies were enumerated after 14 days of growth. n = 2 T
919 cell donors. **** $p < 0.0001$, ** $p < 0.01$, ANOVA with Tukey's multiple comparison
920 correction.
921
922
923

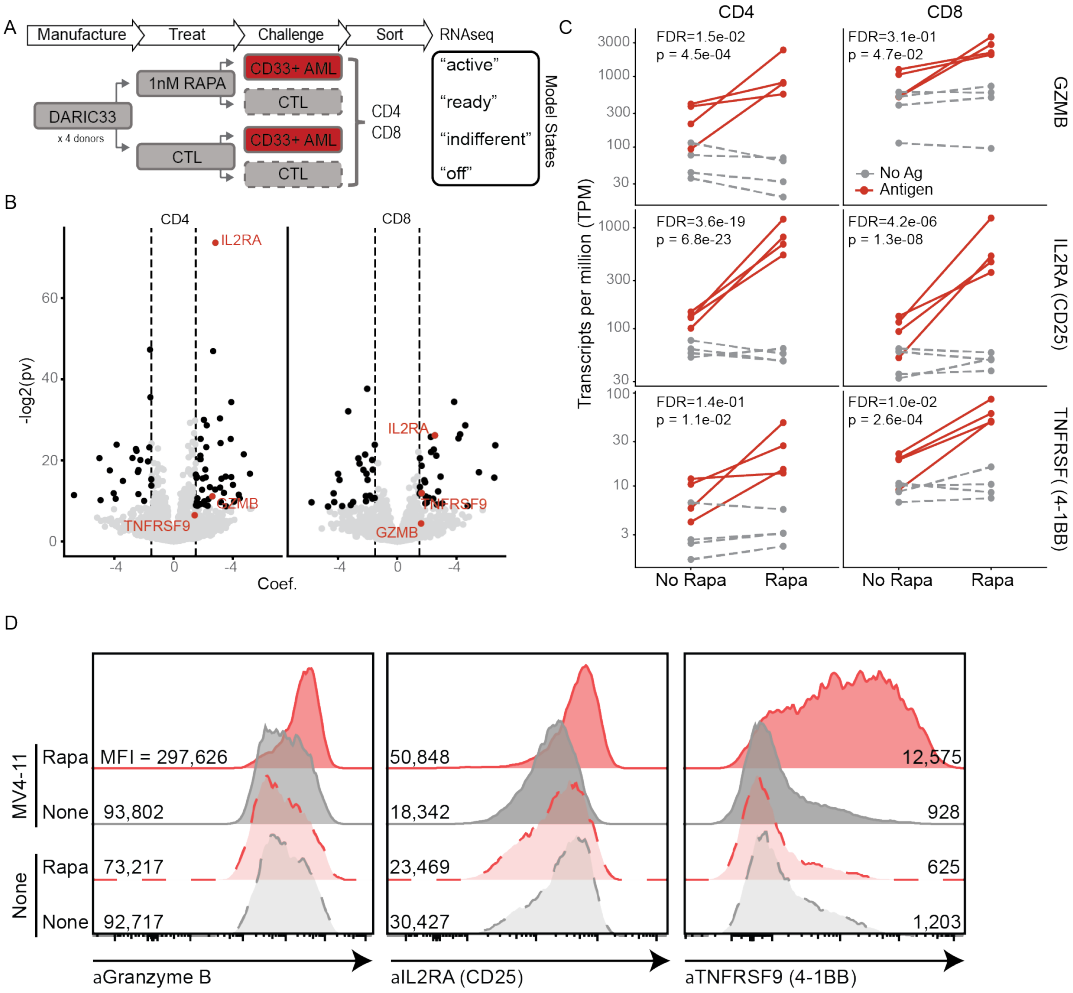

Figure 4. DARIC33 stimulates T cell transcriptional responses in the presence of antigen and rapamycin and without hallmarks of tonic signaling. (**A-D**) DARIC33 cells derived from *n* = 4 healthy donors were incubated with 1nM rapamycin or media alone prior to culture alone or with CD33+ MV4-11 AML target cells. Following coculture, CD4+ and CD8+ cells were sorted and evaluated by RNA-Seq. (**A**) Schema for the experiment. DARIC33 cells resting in the absence of rapamycin or antigen are considered 'off', whereas DARIC33 cells incubated in rapa without antigen and with antigen exposure are labeled 'ready' and 'active' respectively. (**B**) Transcriptional responses among selected genes associated with early T cell activation. (**C**) Volcano plot of the magnitude of statistical significance (*y*-axis) vs magnitude of rapamycin and

antigen (e.g. ‘DARIC active’) effect (*x*-axis, labeled ‘Coef.’ in the figure). GZMB, IL2RA, and TNFRSF9 are shown in red, additional genes exhibiting significant ‘DARIC active’ regulation are shown in black, with more detail provided in a heatmap shown in Fig S5. (**D**) Flow cytometric confirmation that transcriptional changes are reflected in protein abundance. Median fluorescence intensity (MFI) for each sample is shown.

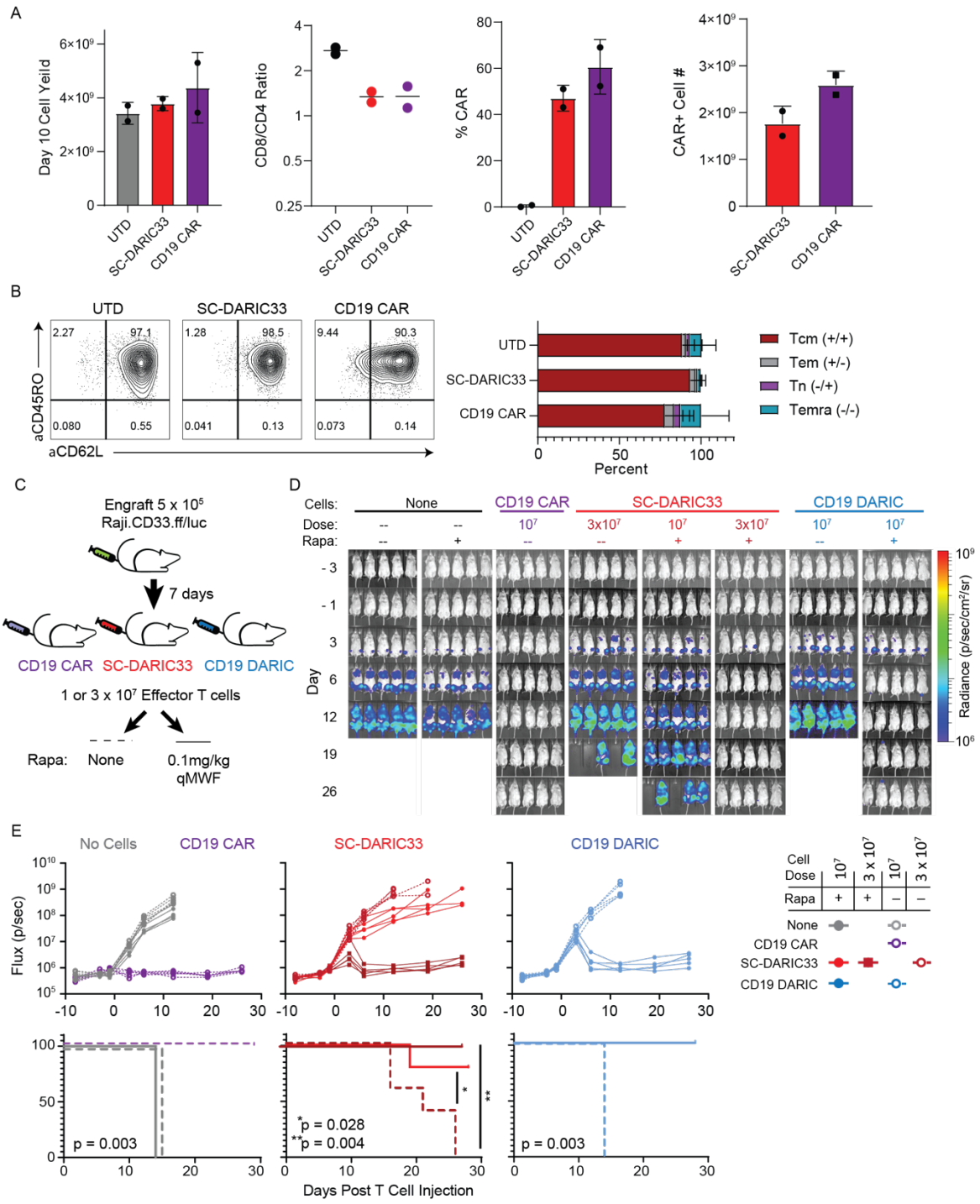

939

940 **Figure 5. Clinically appropriate manufacture of donor matched DARIC33 and CD19 CAR**

941 **allows comparisons of manufacture feasibility and cell potency.** (**A**) Yields of UTD, CD19

942 CAR and DARIC33 cell products following manufacture using reagents and techniques

appropriate for clinical application from *n* = 2 donors. (**B**) Surface expression of CD45RO and CD62L of clinical cell product facsimiles. Representative flow plot is shown *left*, with quantitation from n = 2 donors shown *right* (stacked bars indicate mean ± sd). (**C-E**) 1-3 x 10^7 DARIC33+ cells, CD19 CAR T cells, CD19 DARIC+ cells or an equivalent number of UTD control cells were infused intravenously (IV) in NSG mice 7 days after engraftment of 5 x 10^5 Raji.CD33.ff/luc leukemia cells. Following T cell infusion, mice were treated with 0.1mg/kg rapa 3 times weekly for the indicated durations or were observed. (**C**) Schematic depicting experimental design. To compare cell potency with benchmark immunotherapy products, two doses of DARIC33+ cells were used. (**D**) Tumor progression monitored by bioluminescence, *n* = 5-8 mice per group. (**E**) Quantitation of tumor growth (*above*), with points representing measurements of individual mice. Kaplan Meier survival estimates (*below*), log-rank test *p* values.

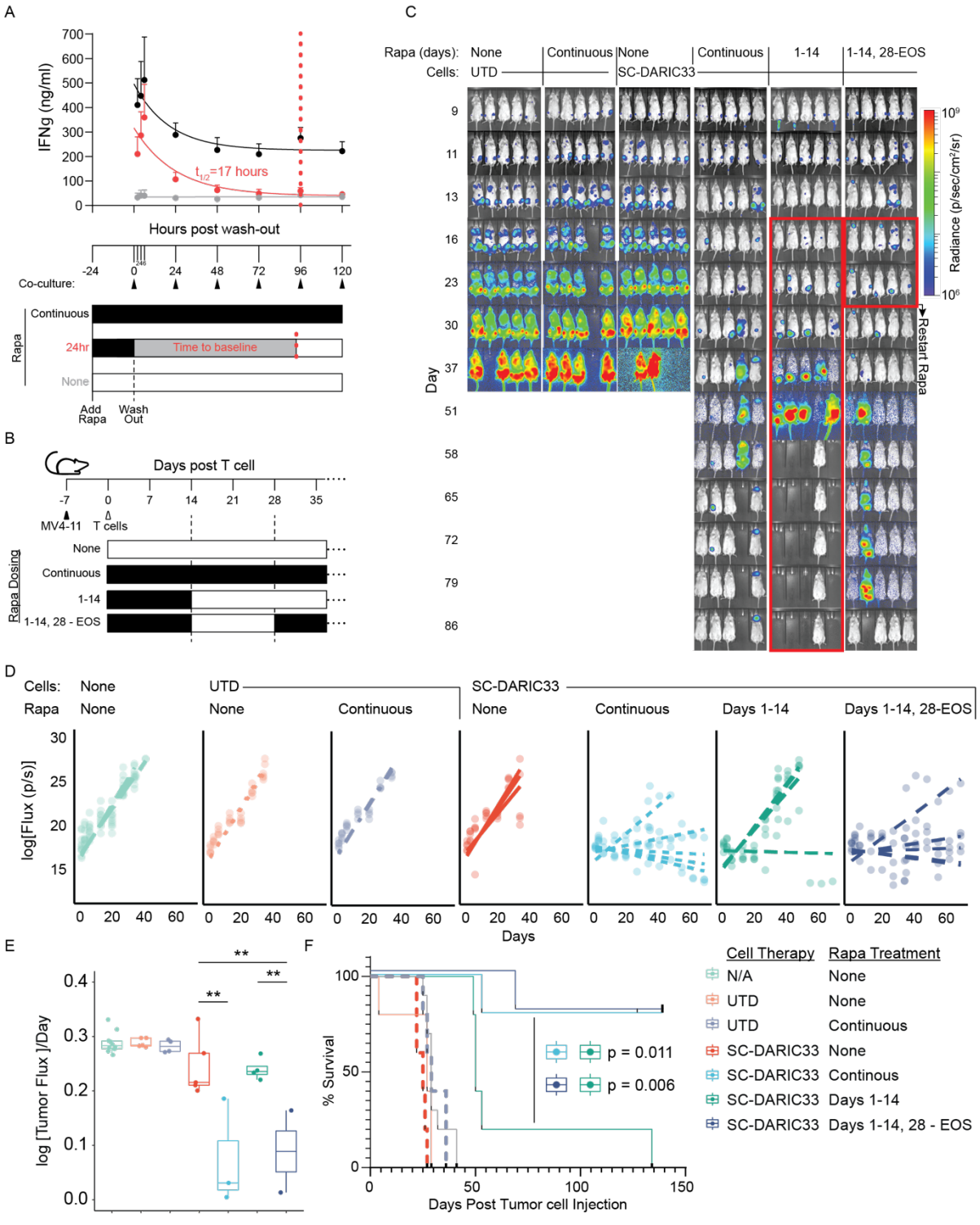

Figure 6. Activation of SC-DARIC33 is reversible. (**A**) DARIC33 cell cytokine responses to antigen at various times following wash out from rapa containing media. DARIC33 cells

replaced into rapa containing media or DARIC33 cells previously cultured in media not containing rapa were used as comparators. The $t_{1/2}$ is determined by fitting a single-phase exponential decay. (**B-F**) 10^7 SC-DARIC33+ cells, or an equivalent number of UTD control cells were infused intravenously (IV) in NSG mice 7 days after engraftment of 1 x 10^6 MV4-11.ff/luc leukemia cells. Following T cell infusion, mice were treated with 0.1mg/kg rapa 3 times weekly for the indicated durations or were observed. (**C**) Tumor progression monitored by bioluminescence, $n = 5$ mice per group. Images taken during a 'pause' in rapa dosing are outlined in red. (**C**) Quantitation of tumor growth. Points are measurements of individual mice, best-fit tumor growth trajectories (see supplemental methods). (**D**) Tumor growth rates. Points are growth rates fit for individual mice, box and whiskers show mean and standard deviation, asterisks indicate ** $p < 0.01$, *t*-tests, with Benjamini-Hochberg correction for multiple comparisons. (**E**) Survival after infusion of DARIC33 cells or UTD cells following by treatment with various rapa schedules. Mantel-Cox log-rank *p* values are shown uncorrected.

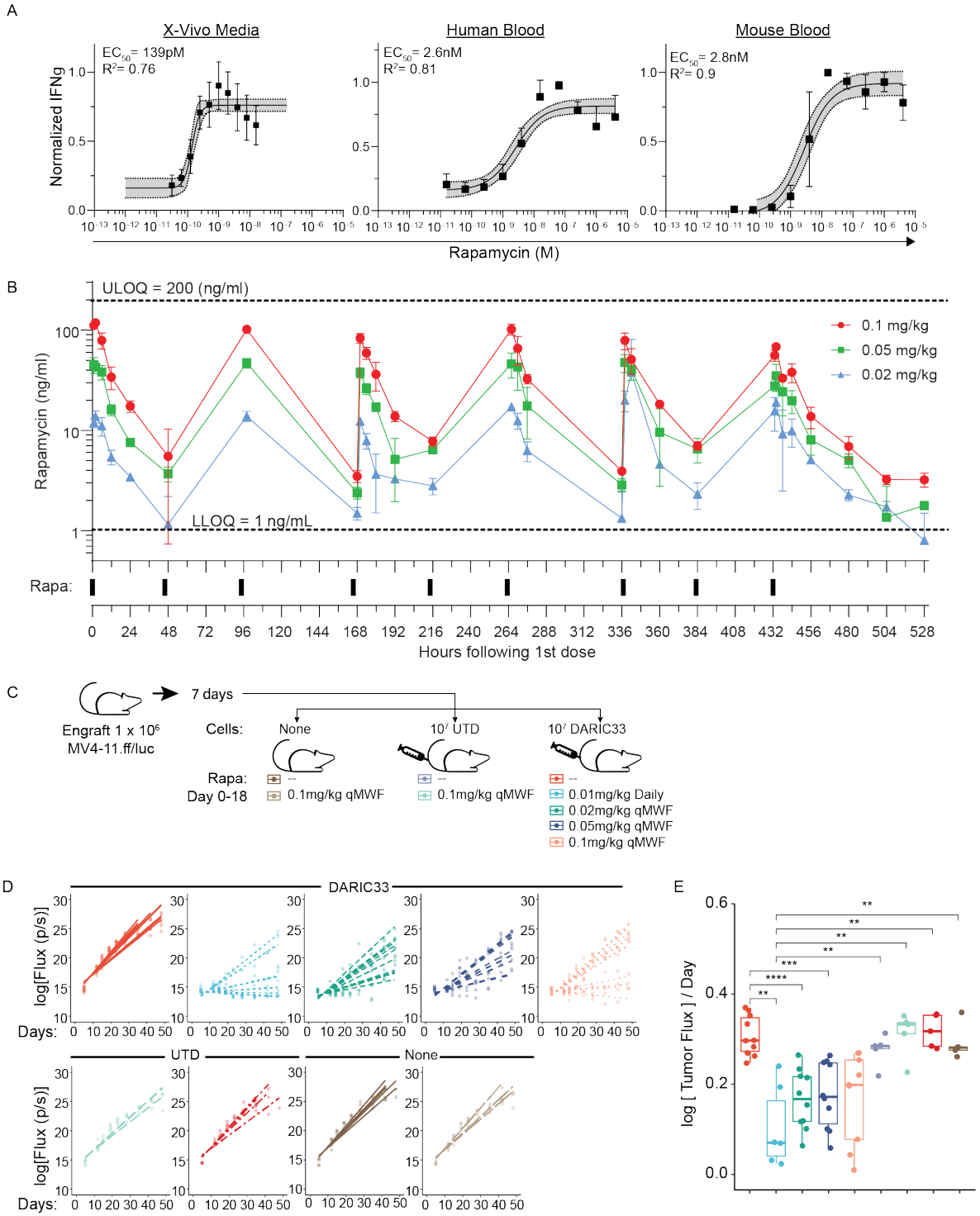

973

974 **Figure 7. In vitro modeling of SC-DARIC33 rapamycin response allows targeted**

975 **rapamycin dosing in vivo.** (**A**) Cytokine release following stimulation of DARIC33 cells with

MV4-11 AML cells in media or whole blood in the presence of increasing rapamycin concentrations. IFNγ responses are normalized per donor and apparent EC50s determined using a four-parameter logistic dose response curves are reported. (**B**) Determination of rapamycin pharmacokinetics in mice. Concentrations of rapa in whole blood obtained during administration of various rapa doses 3 times weekly are shown above, along with the timing of IP rapa injections, *bars, below*. Upper limit of quantitation (ULOQ = 200ng/mL) and lower limit of quantitation (LLOQ = 1ng/mL) are indicated. (**C-D**) AML tumor progression in mice following treatment with DARIC33 and various dose schedules of rapa days 0-18 post T cell infusion. (**C**) Schematic illustrating experimental design. (**D**) Quantitation of tumor growth kinetics. Points represent bioluminescence measures of individual mice (n = 5-10 per group) and lines indicate tumor growth trajectories modeled using linear mixed effects. (**E**) Modeled tumor growth rates (slopes of lines in *D*). Points are growth rates modeled for individual mice, box and whiskers show mean and standard deviation (** $p < 0.01$, *** $p < 0.001$, **** $p < 0.0001$, t-tests with Benjamini-Hochberg correction for multiple comparisons.).

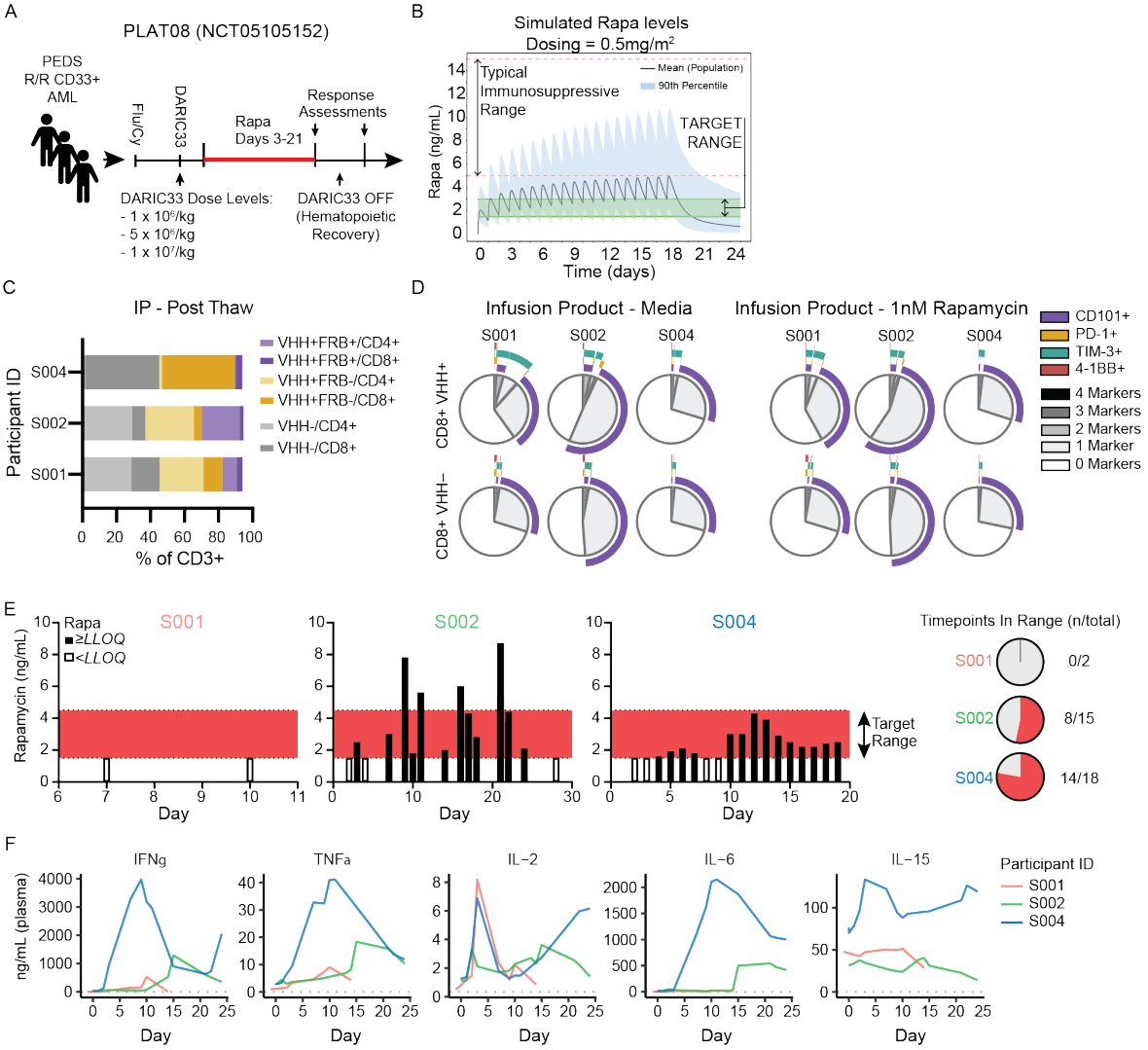

991

992 **Figure 8. Clinical SC-DARIC33 exhibits activity in patients following accurate targeting of**

993 **rapamycin levels.** (**A**) PLAT08 clinical treatment schema. After SC-DARIC33 manufacturing,

994 subjects receive lymphodepletion fludarabine and cyclophosphamide (Flu/Cy) and SC-DARIC33

995 at one of three assigned dose levels on day 0. Rapamycin is administered on days 3-21. Bone

996 marrow biopsies are conducted for response assessments on days 21 and 28. (**B**) Simulated

997 serum rapamycin concentrations using population pharmacokinetic modeling. Daily

998 administration of 0.5mg/m^2 rapamycin achieves trough concentrations above the target range for

SC-DARIC33 activation and peak concentrations below immunosuppressive doses of rapamycin for most pediatric subjects. (**C**) Characteristics of thawed clinical SC-DARIC33 cell products administered to trial participants. The proportion of cells expressing surface DARIC components as assessed by flow cytometry are shown. (**D**) Expression of activation markers by clinical infusion cell products following overnight culture in media alone or media supplemented with 1nM rapamycin. (**E**) Frequent re-evaluation enables successful targeting of serum rapamycin levels in patients. The proportion of timepoints (both peak and trough levels) within the target range (1.5 – 4ng/mL) are shown on the right. (**F**) Elevation of serum cytokines associated with T cell activation is observed following administration of SC-DARIC33. Traces show cytokine levels for samples obtained from each patient. Values reported are the mean of $n = 2$ replicates**.**

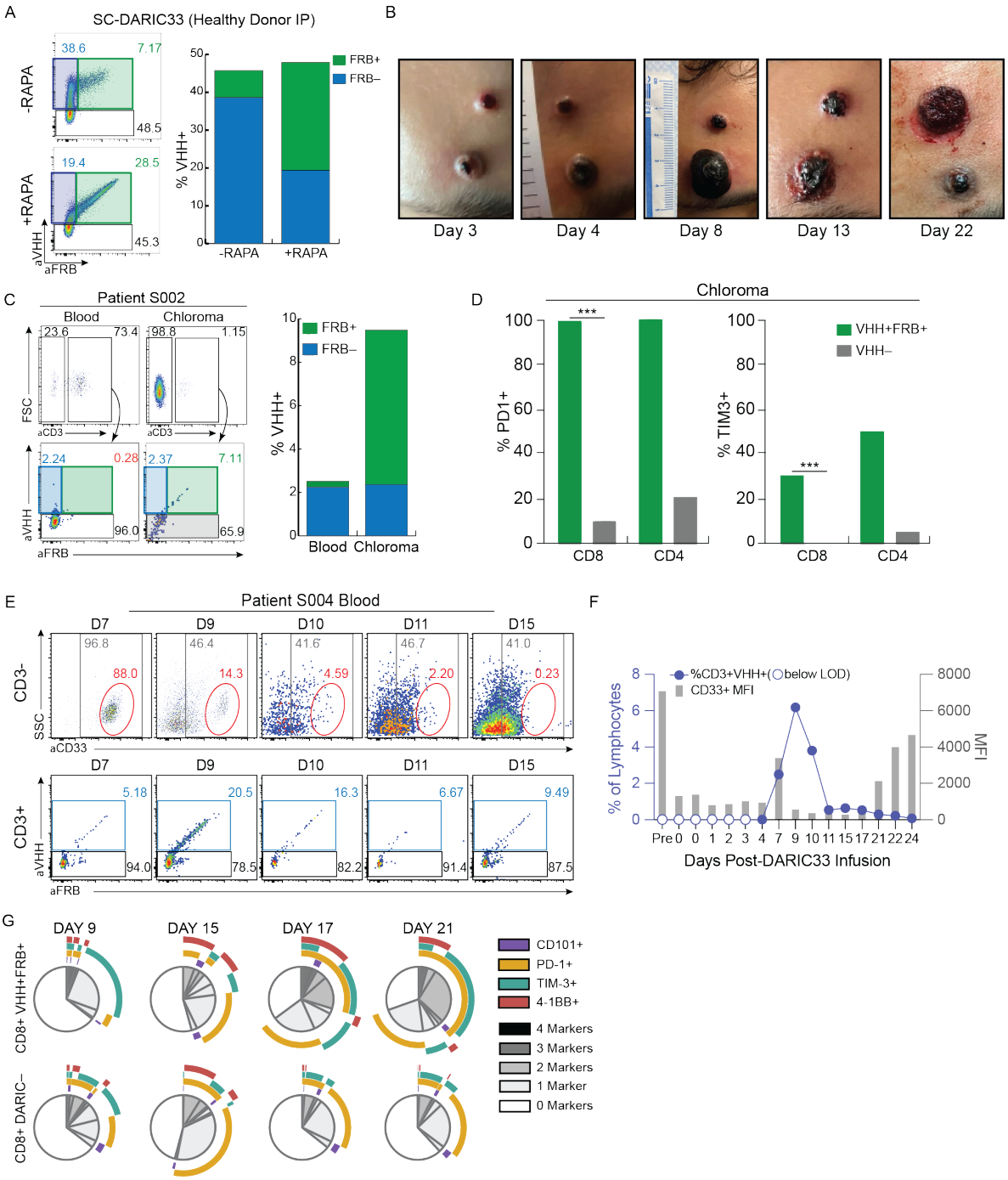

Figure 9. Clinical activity of rapamycin-activated SC-DARIC33 in patients. (**A**) Expression of FRB by SC-DARIC33 is correlated with rapamycin exposure. SC-DARIC33 manufactured from a healthy donor was cultured overnight in media alone or media supplemented with 1 nM

rapamycin. The proportion of VHH+ and FRB+ cells are shown in the bar graph. Note the rightward shift of VHH+ cells following rapamycin exposure. (**B**) Progressive inflammatory changes and hemorrhagic conversion of a chloroma following administration of SC-DARIC33 to subject S002. Samples from chloroma tissues are shown in panels C and D. Photographs with permission. (**C**) Rapamycin-activated FRB+ DARIC33 T cells are expanded within chloroma tissue. Paired blood and chloroma tissue from patient S002 were evaluated by flow cytometry. T cells expressing CD3 were analyzed for VHH and FRB expression. The proportion of VHH+ and FRB+ cells among CD3+ cells are shown in the bar graph. (**D**) Rapamycin-activated DARIC33 cells within chloroma tissue obtained from patient S002 express increased markers of activation including PD1 and TIM3. The proportion of either VHH+FRB+ cells (green bars) or VHH- cells (grey bars) expressing PD1 or TIM3 are shown (*** $p < 0.001$, chi square with Bonferroni correction for multiple tests). (**E**) Peripheral blood from patient S004 shows concurrent expansion of DARIC33 cells and reduction of $CD33^{hi}$ cells. (**F**) Quantification of antigen abundance, as measured by MFI, and expansion of SC-DARIC33 cells within blood samples. Peak SC-DARIC33 expansion is followed by decreased CD33 antigen expression. (**G**) Expression of activation/exhaustion markers by rapamycin-activated SC-DARIC33 cells, as assessed by flow cytometry. Boolean gating results are shown are pie graphs with overlapping arcs indicating multi-antigen expression. At later time points (days 17 & 21), expression of activation markers is increased among VHH+FRB+ cells.